An experimental investigation of wind turbine wakes

Hedda Paulsen Blomhoff

NTNU

Norwegian University
of Science and Technology

Department of Energy
and Process Engineering

EPT-M-2012-22

MASTER THESIS

for

Hedda Blomhoff

Spring 2012

An experimental investigation of wind turbine wakes

En eksperimentell undersøkelse av vindturbin vaker

In wind turbine parks space is normally quite restricted. Although the turbines are normally distributed to reduce the interaction between neighboring turbines, turbine interactions can not be avoided for certain wind directions. There are two main effects. The first is due to the wake behind the turbine. Hence the energy available to downstream turbines is reduced compared to the upstream turbine due to the wind energy consumed by the first. The second effect affecting the downstream turbine is turbulence generated by the upstream turbines. This consists partly of the random turbulence caused by the drag effect from the upstream turbines and partly by the swirl generated from the upstream rotors.

While the wake effect primarily influences the energy output available, the second effect may produce severe dynamic loads on the downstream turbines. The random turbulence will in general produce rather rapid fluctuations that may have a length scale of the order of the chord of the turbine blade and is therefore not very critical since it is likely to have a frequency content which is much higher than the eigenfrequency of the blade. The length scale of the swirling motion is however of the order of the diameter of the rotor and is therefore much more critical for the dynamic behavior of the blade and may cause material fatigue.

The Department of Energy and Process engineering posesses two fully operational model turbines with a rotor diameter of the order of 1m. The turbines are instrumented to allow the power production to be measured directly through the torque and rpm measured off the rotor shaft. In addition the models are equipped with strain gauges to measure the load on the blades.

In this study we like to focus on parameters characterizing the downstream development of the turbine wake. For example: The turbine rotor induces swirl that propagates downstream with the turbine wake, and the turbine tower induces a wind "shadow" that mixes and propagates downstream with the turbine wake and causes asymmetries in the cross-sectional profiles of the wake velocity components.

Within 14 days of receiving the written text on the master thesis, the candidate shall submit a research plan for his project to the department.

When the thesis is evaluated, emphasis is put on processing of the results, and that they are presented in tabular and/or graphic form in a clear manner, and that they are analyzed carefully.

The thesis should be formulated as a research report with summary both in English and Norwegian, conclusion, literature references, table of contents etc. During the preparation of the text, the candidate should make an effort to produce a well-structured and easily readable report. In order to ease the evaluation of the thesis, it is important that the cross-references are correct. In the making of the report, strong emphasis should be placed on both a thorough discussion of the results and an orderly presentation.

The candidate is requested to initiate and keep close contact with his/her academic supervisor(s) throughout the working period. The candidate must follow the rules and regulations of NTNU as well as passive directions given by the Department of Energy and Process Engineering.

Risk assessment of the candidate's work shall be carried out according to the department's procedures. The risk assessment must be documented and included as part of the final report. Events related to the candidate's work adversely affecting the health, safety or security, must be documented and included as part of the final report.

Pursuant to "Regulations concerning the supplementary provisions to the technology study program/Master of Science" at NTNU §20, the Department reserves the permission to utilize all the results and data for teaching and research purposes as well as in future publications.

The final report is to be submitted digitally in DAIM. An executive summary of the thesis including title, student's name, supervisor's name, year, department name, and NTNU's logo and name, shall be submitted to the department as a separate pdf file. Based on an agreement with the supervisor, the final report and other material and documents may be given to the supervisor in digital format.

Department of Energy and Process Engineering, 16. January 2012

Olav Bolland
Department Head

Lars Sætran
Academic Supervisor

Research Advisors: Fabio Pierella

Preface

This master thesis has been performed at the Department of Energy and Process Engineering, at the Norwegian University of Science and Technology, NTNU and will be submitted for the degree: Master of Science. The work was completed within 20 weeks and gave 30 credit points.

First, I would like to thank Professor Lars Sætran for being my supervisor and giving me the opportunity to work with this thesis and to give useful advice throughout the process.

I am most grateful to Fabio Pierella, PhD at the department, for help during the experiments in the wind tunnel and for good feedback and guidance when analyzing the data and during the writing process.

Furthermore, I would like to thank Arnt Kollstad for help when installing the turbine in the wind tunnel and to manufacture the additional tower used in the experiments.

Finally, I would like to thank Heiner Schümann for letting me use his calibration program when evaluating the data.

Hedda Blomhoff

Hedda Blomhoff
Trondheim, 01. Juni 2012

Abstract

In the present study the wake behind a scaled; Horizontal Axis Wind Turbine (HAWT) has been investigated. The experiments were performed at the Department of Energy and Process Engineering, at the Norwegian University of Science and Technology, NTNU.

The turbine was installed in the wind tunnel at the department and measurements were performed at several distances behind the turbine to examine the development of the flow. A five-hole pitot probe was applied as measurement instrument. The instrument made it possible to calculate both size and direction of the velocity components.

Through the experiments, characteristic curves of the turbine and grid measurements over the cross-section of the wind tunnel, were obtained.

The power and thrust coefficients were measured against the local velocity ratio at the tip of the blade, the 'Tip Speed Ratio' (TSR). The power coefficient had a peak at $TSR = 5, 5$. The maximum value at this point was $0, 45$. The highest measured thrust coefficient was $1, 15$, achieved at $TSR = 10, 3$. During the experiments the turbine operated at optimal conditions, at the highest obtained power coefficient.

Measurements behind the turbine found that the axial velocity distribution developed as expected. A significant velocity deficit was measured in the wake behind the turbine, which gradually decreased with increased distance to the turbine. Due to the presence of the hub and tower, the middle of the wake was characterized by disturbances. Moving down the wake the profile got more symmetric. The tangential profile was almost symmetric about the origin, right behind the turbine, but drifted to the left at increased distance downstream. Contribution from the tangential components were gradually reduced further down the wake.

The tower shadow moved with the rotation of the wake, in clockwise direction, as a region of lower velocities than the prevailing wake. Further downstream the tower shadow merged with the surrounding wake.

The rotational axis relocated in the wake behind the turbine. Downstream, measurements showed that the center of rotation moved to the left of the origin. To investigate if the tower was responsible for the experienced downshift, an additional tower was mounted to the tunnel roof, above the turbine. The additional tower created symmetry about the hub and gave a symmetric development of the flow field. Thus, it was concluded that the tower was responsible for the relocation of the rotational axis.

Sammendrag

I dette forsøket er vaken bak en skalert, horisontalakset vindturbin undersøkt. Forsøket ble utført ved Institutt for Energi Prosess og Strømningsteknikk, ved Norges Teknisk - Naturvitenskaplige Universitet, NTNU.

Vindturbinen ble plassert i vindtunnelen ved instituttet og målinger ble gjennomført ved forskjellige avstander bak turbinen, for å undersøke utviklingen av strømmen. Et fem-huls pitotrør ble benyttet som måleinstrument. Instrumentet gjorde det mulig å beregne både størrelse og retning på hastighetskomponentene.

Gjennom forsøkene ble karakteristiske kurver målt og det ble utført grid målinger over tverrsnittet av vind tunnelen.

Den Aerodynamiske virkningsgraden og drivkrafts koeffisienten ble målt mot den lokale hastighetsraten ved tuppen av bladet, 'Tip Speed Ratio' (TSR). Den Aerodynamiske virkningsgraden nådde et høydepunkt ved $TSR = 5,5$. Den maksimale verdien i dette punktet var $0,45$. Den største drivkrafts koeffisienten ble målt til $1,15$, oppnådd ved $TSR = 10,3$. Under forsøkene kjørte turbinen ved optimale forhold, på den maksimale virkningsgraden.

Den aksiale hastighets fordelingen utviklet seg som forventet. En betydelig hastighetsreduksjon ble målt i vaken nedstrøms for turbinen, som gradvis ble mindre med økende avstand til turbinen. Midten av vaken var preget av forstyrrelser i området like bak turbinen, grunnet påvirkning fra tårnet og navet. Videre nedstrøms ble profilen mer symmetrisk. Den tangentielle hastighets profilen var tilnærmet symmetrisk om origo, rett bak turbinen, men forflyttet seg mot venstre ved økende avstand. Den tangentielle komponenten ble gradvis redusert nedover vaken.

Tårnskyggen forflyttet seg i vaken bak turbinen. Nedstrøms viste målingene at senteret for rotasjon forflyttet seg til venstre for origo. For å undersøke om tårnet var årsaken til forflytningen av rotasjonsaksen, ble et ekstra tårn montert til taket i tunnelen, over turbinen. Det ekstra tårnet skapte symmetri om navet og førte til en symmetrisk utvikling av strømningsfeltet. Med dette resultatet, ble det konkludert at tårnet var årsaken til forflytningen av rotasjonsaksen.

Contents

List of Figures

Nomenclature

α Angle of attack $[-]$

$\dot{V}$ Volumetric flow rate $[m^3/s]$

Γ Total circulation $[-]$

λ_r Local velocity ratio $[-]$

Ω Angular velocity $[rpm = 1/min]$

ω Angular velocity transferred to airflow $[rpm = 1/min]$

$\vec{U}$ Velocity vector $[m/s]$

ϕ Yaw angle $[-]$

π Pi $[-]$

ρ Density $[kg/m^3]$

θ Roll angle $[-]$

$\triangle p_{contr}$ Contraction pressure $[N/m^2]$

$\triangle \Gamma$ Circulation generated at each blade $[-]$

A Area $[m^2]$

a Induction factor $[-]$

a' Tangential induction factor $[-]$

A_1 Area at inlet of contraction $[m^2]$

A_2 Area at outlet of contraction $[m^2]$

B Systematic uncertainty

C_p Power coefficient $[-]$

C_T Thrust coefficient $[-]$

D Drag force $[N]$

D Diameter $[m]$

E Kinetic energy $[m^2/s^2]$

F Function of n measured variables

g Acceleration of gravity $[m/s^2]$

$h_{alcohol}$ Height of alcohol $[m]$

K Number of blades $[-]$

L Lift force $[N]$

M Pitching moment $[Nm]$

m Mass $[kg]$

N Number of samples $[-]$

P Power $[Nm/s]$

p Pressure $[N/m^2]$

p_1 Pressure at inlet of contraction $[N/m^2]$

p_2 Pressure at outlet of contraction $[N/m^2]$

p_∞ Pressure in free stream $[N/m^2]$

p_{atm} Atmospheric pressure $[N/m^2]$

p_a Pressure behind disc $[N/m^2]$

p_b Pressure in front of disc $[N/m^2]$

Q Torque $[Nm]$

R Radius at tip of blade $[m]$

r Radius $[m]$

$R_{spesific}$ Gas constant $[Nm/kgK]$

rms Root Mean Square $[-]$

S_i Standard deviation

T Thrust force [N]

T_{temp} Temperature [K]

TSR Tip Speed Ratio [$-$]

U Velocity [m/s]

U_1 Velocity at inlet of contraction [m/s]

U_2 Velocity at outlet of contraction [m/s]

U_∞ Free stream velocity [m/s]

U_i Velocity i [m/s]

U_m Mean velocity [m/s]

U_n Velocity at hole n at the five-hole pitot probe [m/s]

U_t Tangential velocity [m/s]

U_w Velocity in wake [m/s]

U_x Velocity in x direction [m/s]

U_y Velocity in y direction [m/s]

U_z Velocity in z direction [m/s]

W Uncertainty intervall

Chapter 1

Introduction

In search of new and renewable sources of energy, wind production is one of the most promising areas of development. Arrangements of wind turbines in wind farms increase the energy production. The first wind farm was developed in 1970 in California, United States. In Europe the development of wind farms started in 1980 in Denmark. Today Denmark, Germany, Spain and the Netherlands are the leading European countries in the wind industry [17]. At times energy produced by wind, in Western Denmark and parts of Germany, exceeds power demand and they are able to export power produced by wind [24]. Since wind is both a clean, free and practically unlimited source of energy, production of energy by wind farms is one of the cheapest forms of renewable technologies available today [20].

In a wind farm turbines are placed in defined structures to produce the greatest amount of energy. Across a wind farm the different turbines will experience different wind conditions which results in different power production. The first row of turbines will experience the best premises because they are not disturbed by the wakes from other turbines. Turbine wakes affect the power production in two different ways; by velocity deficits and increased turbulence intensity [10]. Wind turbines utilize the kinetic energy in the wind to produce energy. In the presence of velocity deficits, less energy will be produced by the downstream turbines [17].

To optimize the power production in a wind farm the objective is to obtain a layout, with respect to array losses, that produce the highest amount of energy [10]. The question is where to locate and how close to space the turbines. Optimizing the siting can make a great difference to the total power production. Due to interaction between the neighboring turbines, it is desirable to understand the development of the wake to achieve the best possible performance. The wake is a complex structure and consists of several unknown parameters, such as the velocity components with respect to size and direction and the turbulent behavior. Several studies have focused on the development of the wake downstream of a turbine, e.g. Bartl [5], Blomhoff [6], Nygard [22], Talmon [28, 29] and Maeda et al. [16]. The results from these studies assume that the center of rotation moves below the rotational origin, moving further away from the turbine. A proposed explanation for the relocation of the rotational axis is contribution from the

tower.

The objective of this experimental study is to investigate the development of the wake, with emphasis on the experienced downshift of the rotational axis and the development of the tower shadow. The aim is to figure out if the tower is the reason for the downshift and how strong the contribution from the tower shadow is further downstream of the turbine:

- Cross-sectional measurements behind a single turbine, at different distances downstream, are performed to investigate the propagation of the tower wake. The performance of the turbine is also examined.

- An additional tower, equal to the turbine tower, is mounted to the tunnel roof to create symmetry about the hub. Measurements over the cross-section are performed at different distances downstream of the rotor, to investigate the contribution of the turbine tower to the relocation of the rotation.

- To examine the strength of the tower shadow, measurements across the wake are accomplished at a lower wind turbine velocity and at a lower wind tunnel rotational speed. The experiments are performed both with and without the additional tower and the turbine is operating at optimal conditions.

The experiments are performed in the large wind tunnel at The Department of Energy and Process Engineering, at the Norwegian University of Science and Technology, NTNU. The development behind a scaled; Horizontal Axis Wind Turbine (HAWT) is examined with a five-hole pitot probe as measurement instrument. This instrument makes it possible to evaluate the flow pattern with velocity components in axial, radial and tangential direction.

In the first part of this paper, theory about the aerodynamics of wind turbines and a description of the experimental set-up are introduced. In the second part of the thesis, results from the experiments and discussion of the obtained results are presented.

The results from this experimental study will hopefully give a better understanding of the development of the wake and contribute to future planning and improvement of wind farm technology.

Chapter 2

Aerodynamics of Wind turbines

In this chapter, theory about the aerodynamics of wind turbines will be presented. Forces acting on the turbine, performance characteristics, expected development of the flow downstream of the turbine and arrangement of wind turbines in wind farms will be looked into.

A wind turbine produces energy by utilizing the kinetic energy in the wind:

$$E = \frac{1}{2}mU^2 \tag{2.1}$$

As the air approaches the rotating blades the velocities decreases. The airflow not passing the rotating area is slightly influenced by the rotation. Surrounding the affected airflow an imaginary control volume, with a circular cross-section, can be constructed. The actuator disc theory is a simplified model explaining the forces acting on the turbine, the power produced and the effect of the rotor on the development of the airflow downstream of the turbine.

Some assumptions for the actuator disc theory to be valid, according to Manwell et al. [17] are:

- homogenous, incompressible, steady flow

- no frictional drag

- an infinite number of blades

- uniform thrust over the rotor area

- no rotation in the wake

- the pressure far upstream and far downstream is equal to the atmospheric pressure

Figure 2.1 below, illustrates the actuator disc theory.
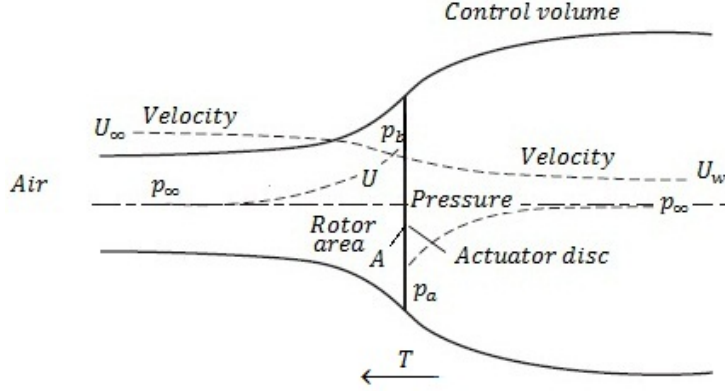
Figure 2.1: Simplified actuator disc model [7] (modified)

Because the disc obstructs the airflow, the pressure increases as the flow approaches the disc, p_b. This results in a decrease in velocity before the air passes the turbine blades. The velocity in this area U, is lower than the free stream velocity, U_∞. To obtain the assumption of steady state flow, $(\rho A U)_\infty = (\rho A U)_w$, the cross-sectional area must expand.

When the air passes the disc the static pressure, p_a, will drop below atmospheric pressure, p_∞, as can be seen in figure 2.1. The velocity development will not experience this abrupt change past the disc, but will gradually be reduced as the pressure drop recovers. The area behind the rotating blades is referred to as wake, U_w.

2.1   Axial Forces

By assuming constant density, neglected viscosity, smooth, frictionless and incompressible flow, Navier Stokes equation is simplified to Bernoulli's equation [33]. The equation is used to evaluate the pressure distribution over the rotor and to calculate the pressure in the wake. Continuity and conservation of mass assumes that the pressure in the free flow, before interaction with the rotor area, is equal to the pressure further downstream of the turbine where stable conditions are reestablished.

Under these idealized assumptions the following relationship is determined:

$$p_\infty + \tfrac{1}{2}U_\infty^2 = p_b + \tfrac{1}{2}U^2 \tag{2.2}$$

$$p_a + \tfrac{1}{2}U^2 = p_\infty + \tfrac{1}{2}U_w^2 \tag{2.3}$$

The thrust force, T, acts on the rotating disc as a counter force to the forces in the wind. By using equation 2.2 and 2.3 above, the thrust force is expressed as:

$$T = (p_b - p_a) \times A = \tfrac{1}{2}\rho(U_\infty^2 - U_w^2) \times A \tag{2.4}$$

10

The axial induction factor is defined as the relationship between the decrease in velocity towards the rotating disc and the velocity in the free flow:

$$a = \frac{U_\infty - U}{U_\infty} \tag{2.5}$$

The relationship between the induction factor and the velocity in the wake is:

$$U_w = U_\infty(1 - 2a) \tag{2.6}$$

Combining 2.5 and 2.6 we get the following expression for the thrust force:

$$T = \tfrac{1}{2}\rho A U_\infty^2 (4a(1 - a)) \tag{2.7}$$

The thrust force acting on a small element of the blade, dr, can be described as:

$$dT = \rho U_\infty^2 (4a(1 - a)\pi r dr) \tag{2.8}$$

2.2 Rotational Forces

Figure 2.1 shows the idealized actuator disc concept with the assumption of a non-rotating wake. In reality the airflow passing the rotor area creates a torque on the blades. Due to the torque, the blades move with an angular velocity, Ω, about an axis normal to the disc and parallel to the free stream. This is illustrated in figure 2.2. A counter force is created with equal strength, but in opposite direction, on the wind [7]. This counter force makes the airflow, after passing the disc, move in opposite direction of the blades. The velocity of the air particles gets a tangential and radial component. The rotation maintains further down the wake.
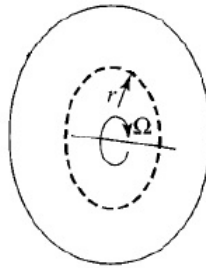

Figure 2.2: Rotor disc with angular velocity, Ω, and local radius, r [7]

The angular velocity increases over the blades and the angular velocity alters to $\Omega + \omega$, while the axial velocity remains the same [17]. ω is the velocity transferred to the airflow. Change in tangential velocity can then be expressed with a tangential induction factor:

$$a' = \frac{\omega}{2\Omega} \tag{2.9}$$

The blades rotate with a local velocity of Ωr. The thrust force acting on an element of the blade is expressed as:

$$dT = 4a'(1 + a')\rho\Omega^2 r^3\pi dr \tag{2.10}$$

Combining equation 2.8 and 2.10 we get the local velocity ratio:

$$\lambda_r = \frac{\Omega r}{U_\infty} \tag{2.11}$$

The local velocity ratio for the tip of the blade is referred to as the Tip Speed Ratio (TSR). The Tip Speed Ratio is defined as the relationship between the velocities at the tip of the blade, where the radius is the length of the blade, R, and the velocity in the free flow:

$$TSR = \frac{\Omega R}{U_\infty} \tag{2.12}$$

2.3   Performance characteristics

A way to classify the performance of a wind turbine is by the power coefficient, C_p. The power coefficient describes the relationship between the power extracted by the turbine and the power available in the wind through the rotor area:

$$C_p = \frac{Rotor Power}{Power In The Wind} = \frac{P}{\sfrac{1}{2}\rho U_\infty^3 A} \tag{2.13}$$

Betz limit is the maximum power a wind turbine can extract from the wind under idealized conditions, i.e. the actuator disc theory previously described. The Betz limit was derived by Albert Betz in 1919 and is a number to compare with the actual performance of real wind turbines, $C_p = \frac{16}{27} = 0,593$ [10]. Due to rotation of the wake, a finite number of blades, related tip losses and non-zero aerodynamic drag the $C_p$value of operating turbines will not be able to reach the value of Betz limit [17].

The power produced by the rotor is determined as: $P = Q\Omega$. Q represents the torque on the element. Plotting the C_p against the Tip Speed Ratio (TSR), equation 2.12, we obtain the turbine performance curve: a typical example is illustrated in figure 2.3.
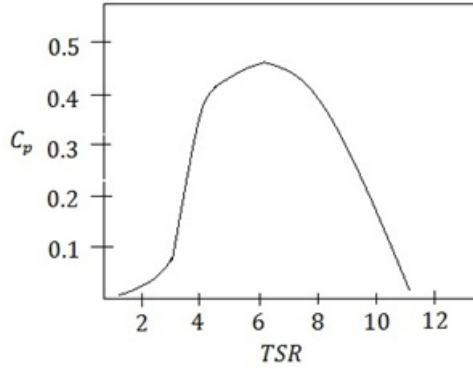
Figure 2.3: C_p- TSR curve

In the figure the optimal operating condition is given at a certain TSR value. Here the energy efficiency is evenly distributed and the power production is optimized. It is desirable to let the turbine work in this area. If the value is lower than optimal the angle of attack is high, which results in stalled conditions. In this TSR region the wind will pass the rotor with less interaction with the turbine blades. The power is reduced and the power coefficient will decrease as a result. At higher rotational speed the power coefficient decreases, due to a low angle of attack and resulting drag effects [7]. The highest achieved TSR value is called the 'runaway TSR'. At this value the turbine is no longer able to produce power.

Another parameter used to evaluate the performance of the turbine is the thrust coefficient. The thrust coefficient is defined as the axial thrust force divided by a dynamic force, both acting on the rotor area.

$$C_T = \frac{ThrustForce}{DynamicForce} = \frac{T}{\frac{1}{2}\rho U^2 A} \tag{2.14}$$

A typical development of the thrust coefficient is sketched in figure 2.4.
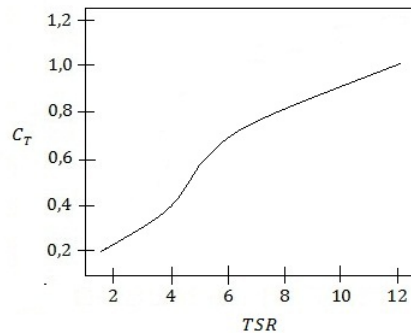
Figure 2.4: C_T- TSR curve

With increasing Tip Speed Ratio the value of the thrust coefficient grows. At

higher rotational speed the disc becomes more "solid" and the air will not be able to flow through the rotor. Instead the air will flow around the disc and there will be separation behind the rotor, similar to the behavior behind a solid disc. This results in a higher thrust force acting on the turbine [7]. In figure 2.4 there is a slightly inflection of the curve. This is experienced because the turbine is working in the transition area between stalled and optimal conditions.

2.4 Aerodynamics of the blade

The blades of a wind turbine are designed to utilize the kinetic energy in the wind. The goal in the design process is to maximize the energy capture of the rotor, to achieve a maximum power coefficient [7]. The shape of the cross-section of the blade is equal to the form of an airfoil.

There are two main forces and one moment acting on the turbine blade: lift, L, and drag, D, forces and pitching moment, M. The lift force acts perpendicular to the direction of the airflow and is due to the different pressure distribution between the top and the bottom of the airfoil surface. The drag force acts parallel to the direction of the airflow. The drag force is a result of the pressure distribution on the surface, toward and away from the oncoming flow, and the viscous friction forces acting at the surface of the airfoil. The pitching moment acts about an axis perpendicular to the cross-section of the airfoil [17]. The forces and the moment, as well as the angle of attack are shown in figure 2.5. The angle off attack, α, is the angle which the air strikes the blade.
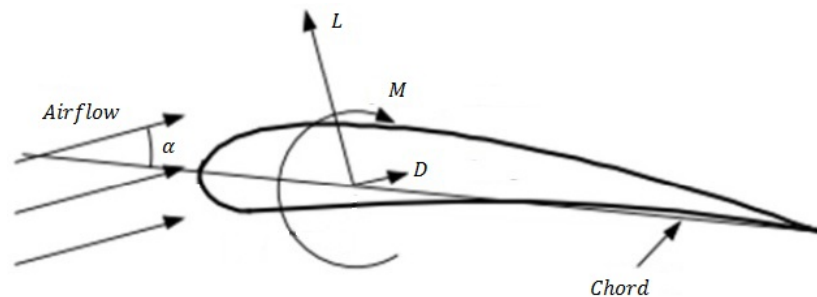
Figure 2.5: Lift, drag and pitching moment acting on airfoil [17] (modified)

The pressure gradient may be directed in the same, or in the opposite direction of the airflow. The flow in the boundary layer is slowed, either by the pressure gradient or the surface friction. Stalled conditions are attained if the boundary layer is stopped or reversed. In this case the boundary layer is separated from the airfoil, the lift force decreases and the drag force increases. Stall occurs when the angle of attack exceeds a certain value, resulting in separation of the boundary layer at the upper surface of the airfoil. This condition may happen at certain blade locations or when the wind turbine is operating at certain conditions, such as too high or two low rotational speed (see

chapter 2.3). An airfoil acting under stalled conditions is sketched in figure 2.6. In the figure the boundary layer is no longer attached to the airfoil at the upper surface.
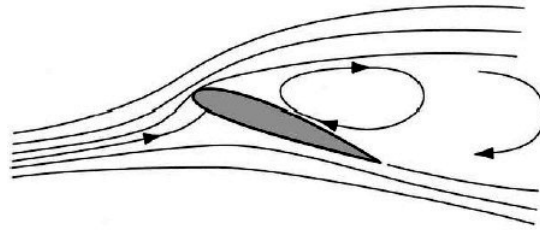
Figure 2.6: Airfoil acting at stalled condition [7]

2.5 Wake development

The wake can be divided into two sections. The near and the far wake. The transition area between the two divisions is approximately one rotor diameter downstream of the rotor [26]. The geometric properties of the rotor determine the flow field in the near wake. In the far wake, the shape of the rotor is less important.

The actuator disc theory assumes that the control volume, surrounding the wake, separates the free flow from the flow in the wake entirely. In reality this is not the case. In the transition area between the wake and the free flow, a shear layer is created due to the velocity difference. The shear layer expands until it reaches the wake axis, as illustrated in figure 2.7. This point represents the end of the near wake. In the shear layer, turbulent eddies are formed when the kinetic energy in the wind is separated into thermal energy. Turbulence in the wake mixes the lower velocities in the wake with the higher velocities in the free stream and transfers momentum into the wake. This contributes to the expansion of the wake and a reduction in the velocity deficit [26].
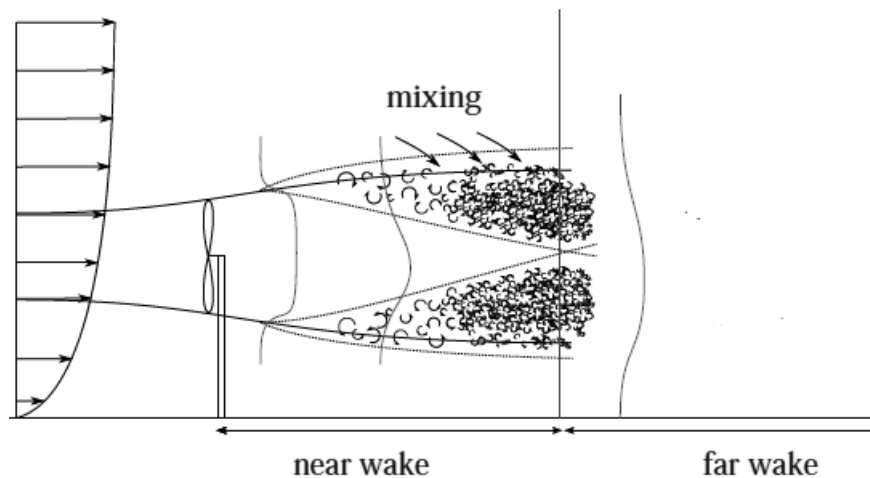
Figure 2.7: Transition between the near and far wake [26] (modified)

In the far wake the velocity deficit gradually decreases and the turbulent level is predominant. Here the wake is fully developed.

The axial velocity, parallel with the free stream, is close to symmetric across the rotational axis. The velocity distribution in the wake is considerably lower than the velocity in the free stream. This is due to the pressure reduction over the rotating plane, previously described. A potential axial velocity distribution is illustrated in figure 2.8. Here the velocity, U, is non-dimensionalized by the velocity in the free flow, U_∞.
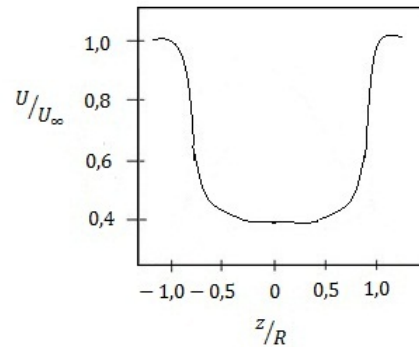
Figure 2.8: Axial velocity distribution

Rotation in the wake contributes to the tangential velocity distribution. Each blade generates a radial, uniform circulation with strength $\triangle\Gamma$. This tip vortex is created due to the pressure difference between the upper and lower side of the blade. A helical vortex is then generated from the tip of each blade, with equal strength, moving down the wake with the local velocity. In the center of rotation, a root vortex of strength $\Gamma = K \times \triangle\Gamma$, is formed. K is determined by the number of blades. The circulation maintain downstream of the turbine and is the main contributor to the tangential velocity profile. Figure 2.9 demonstrates how the circulation evolves downstream of a turbine that rotates clockwise, with the airflow rotating counter clockwise.
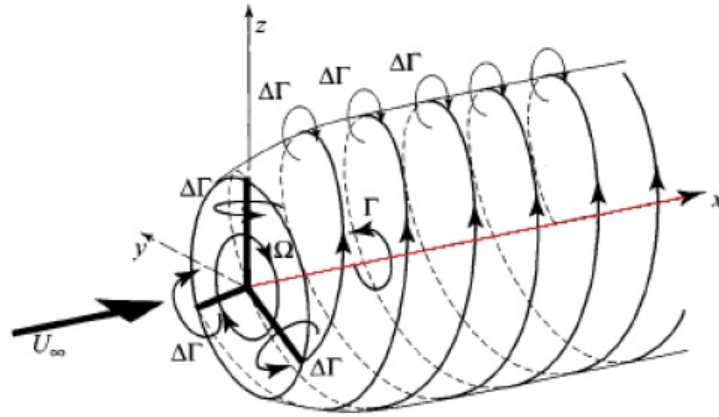
Figure 2.9: Circulation in the wake [7] (modified)

The dimensions of the tangential velocity components are reduced with increased radius and get close to zero at the outer edge of the control volume. There is almost no circulation in the center of rotation, resulting in small tangential components. However, the tangential velocity enhance with reduced radius. Thus, in close distance to the rotational axis, the contribution from the circulation is severe and large tangential components are formed. Figure 2.10 shows the expected tangential velocity distribution over the cross-section, at hub height, when the wake rotates in clockwise direction.
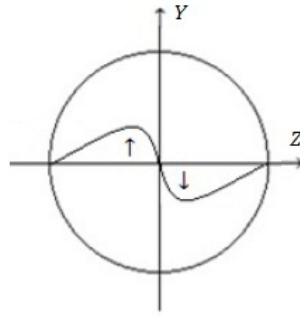
Figure 2.10: Tangential velocity distribution

The radial components point towards the center of rotation to balance the centrifugal forces on the rotating flow. Consequently, measurements in hub height are assumed to have small radial components. This is because the velocity vectors are expected to have almost vertical components in this area.

2.6 Wind farms

When arranging wind turbines in wind farms the question is how to place the turbines to get the best power output available. There will be interaction between the different turbines due to turbulence, rotation and wake development. Array losses will occur because the wake of the upstream turbines will influence the power produced by the downwind turbines.

Velocity deficits and generation of turbulence are the most important contributors to losses of energy production [20]. The wake consists of velocity deficits and swirling vortices due to interaction between the wind and the rotor surface and different flow patterns over the surface of the blade [17]. Down the arrays in a wind farm the level of turbulence increase, resulting in better turbulence mixing in the wake of the downstream turbines. Consequently, the wake of a downstream turbine recovers more quickly than the wake of a turbine further upstream [26].

In a wind farm, the first row will produce the greatest amount of energy compared to the turbines further down the arrays. The performance of the downstream turbines will be reduced due to extraction of energy upstream. An extensive investigation of the Horns Rev Offshore Wind Farm was performed by Méchali et al. [18]. The wind farm is located close to Denmark, in the North Sea. The study found that: "The general tendency is a large drop from turbine 1 to turbine 2 and a steadily decreasing power output along the line of turbines" [18]. Bartl [5] performed a wind tunnel experiment where the performance of a second turbine, placed downstream of another, was investigated. The experiment found that the obstructed turbine produced only 31% of the power produced by the unobstructed turbine.

Another result of higher turbulence intensity is higher wind velocities and more extreme wind changes over shorter periods. Increased turbulence creates random fluctuations in the load, power output and stresses the entire turbine structure. Consequently, the life of the downstream turbines is reduced.

Energy production by wind turbines, in an economic perspective, is a tradeoff between space and power output. The objective is to obtain a layout producing the highest amount of annual energy, while taking constrains such as wake losses into account. An improved ability to predict wake losses and the wake development, may improve the design of large wind farms significantly.

Experiments in real wind farms are difficult to perform due to vulnerability to atmospheric turbulence, wind shear from the ground effect, wind directions that change both in time and space and effects from the wake of surrounding turbines [30]. Thus, it is difficult to capture all the different parameters in a real wind farm. However, a wind tunnel experiment will give a good indication of the development of the different parameters, even though the experiments are performed under idealized conditions. Consequently, reproduction of several aspects in real situation of the atmospheric and environmental conditions, are problematic.

Chapter 3

Experimental set-up

This chapter contains an introduction of the equipment's used in the experiments and a description of the different set-ups.

3.1 Equipments

3.1.1 Wind Tunnel

The wind tunnel used in the present study is a low-speed, closed return wind tunnel that consists of an $11m$ long test section with height $1,9m$ and width $2,7m$. In figure 3.1 an illustration of the wind tunnel is shown, with a caption on the test section where the experiments were performed.
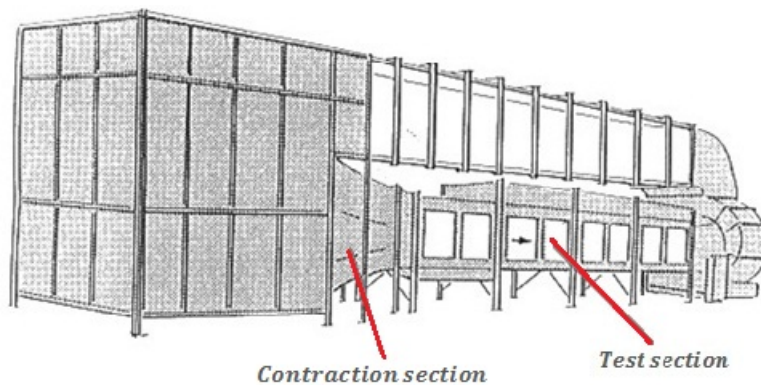
Figure 3.1: Wind tunnel [13] (modified)

A $220kW$ fan produces the wind in the tunnel. Wind velocities in the test section can be adjusted up to $30^{m}/_{s}$. Through a contraction section the velocities are determined. The velocity profile at the inlet is uniform, with a low degree of turbulence [1]. In addition to the contraction section, the tunnel is provided with a force balance and a traverse system.

3.1.1.1 Inlet contraction

The wind tunnel contains a contraction section, before the air enters the test section. As the cross-sectional area decreases, the static pressure is reduced and the velocity at the outlet increases. Pressure holes are encircling the airflow at the inlet and at the outlet of the contraction area, measuring the static pressure at these points. Figure 3.2 gives a schematic representation of the contraction section.
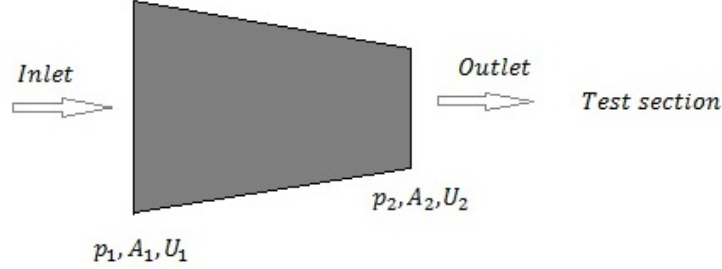
Figure 3.2: Inlet contraction

With known areas and pressures, the velocity at the outlet of the contraction area can be calculated. This is the same velocity as the inlet velocity to the test section. U_2 can be measured from the relationship between the volumetric flow rate through the contraction, equation 3.1, and Bernoulli's relationship, equation 3.2:

$$\dot{V} = U_1 A_1 = U_2 A_2 \tag{3.1}$$

$$p_1 - p_2 = \frac{\rho}{2}(U_2^2 - U_1^2) \tag{3.2}$$

$$U_2 = \sqrt{\frac{2(p_1 - p_2)}{\rho\left(1 - \left(\frac{A_2}{A_1}\right)^2\right)}} \tag{3.3}$$

The ratio between the inlet and the outlet area of the contraction section of the present wind tunnel is:

$$\frac{A_2}{A_1} = \left(\frac{1}{4,36}\right) \tag{3.4}$$

3.1.1.2 Force balance

A six-component force balance is located underneath the test section of the wind tunnel. When measuring the thrust force acting on the turbine, the turbine was fixed to the balance. The force balance can be rotated 180 degrees in both directions, according to the direction of the airflow. In every set-up the turbine was aligned with the flow.

Consequently there was only need for calibrating one component. To calibrate the force balance, weights were added to the respective component and force values were logged. A relationship between the additional weights $[N]$ and volt signals $[V]$, recorded in LabVIEW, was created.

3.1.1.3 Traverse system

To be able to take measurements over the cross-section, a traverse system is fitted in the tunnel. The traverse system is computer controlled and provided with three axes, which makes it possible to take measurements at almost any position in the tunnel. A LabVIEW routine developed by Schümann [27] makes the traverse system move automatically, taking measurements at a given grid. The grid expands from -820 to $+820$ in z-direction and -800 to $+800$ in y-direction as shown in figure 3.3. The grid is refined in areas where steep velocity, turbulence and pressure gradients are expected [27]. The traverse moves into position when the program is started, a sample is taken before the traverse moves to the next measuring point. It is also possible to move the traverse manually from the computer, deciding the next position of the measurements.
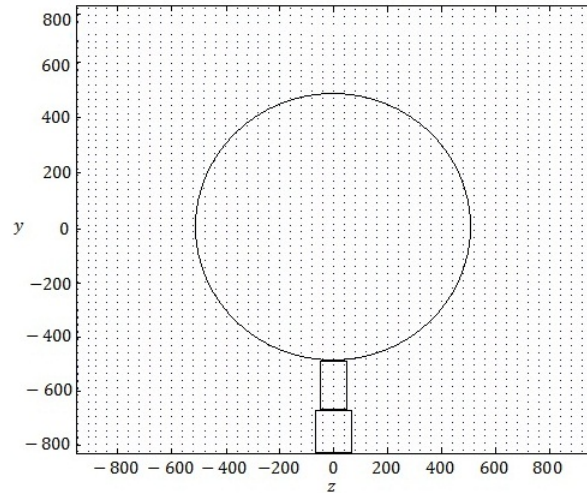
Figure 3.3: Grid of cross-section

3.1.2 Scaled; Horizontal Axis Wind Turbine

A scaled; Horizontal Axis Wind Turbine (HAWT) was applied in the experiments. The rotational diameter of the blades is $0,9m$ and the hub has a diameter of $0,09m$. The turbine tower is $0,95m$ high with a non-uniform diameter.

The rotational velocity is adjusted by a SIEMENS MICROMASTER 440 frequency inverter connected to a $0,37kW$ SIEMENS DC electric motor, placed at the wind tunnel floor. At the end of the shaft of the rotor, a belt is mounted to operate the rotor from the electric motor. The frequency inverter is placed on the outside of the tunnel and the rotational velocity is controlled from here.

In figure 3.4 the turbine is shown from the front, figure 3.4a, and from the back, figure 3.4b. Here the belt mounted to the end of the shaft is visible.
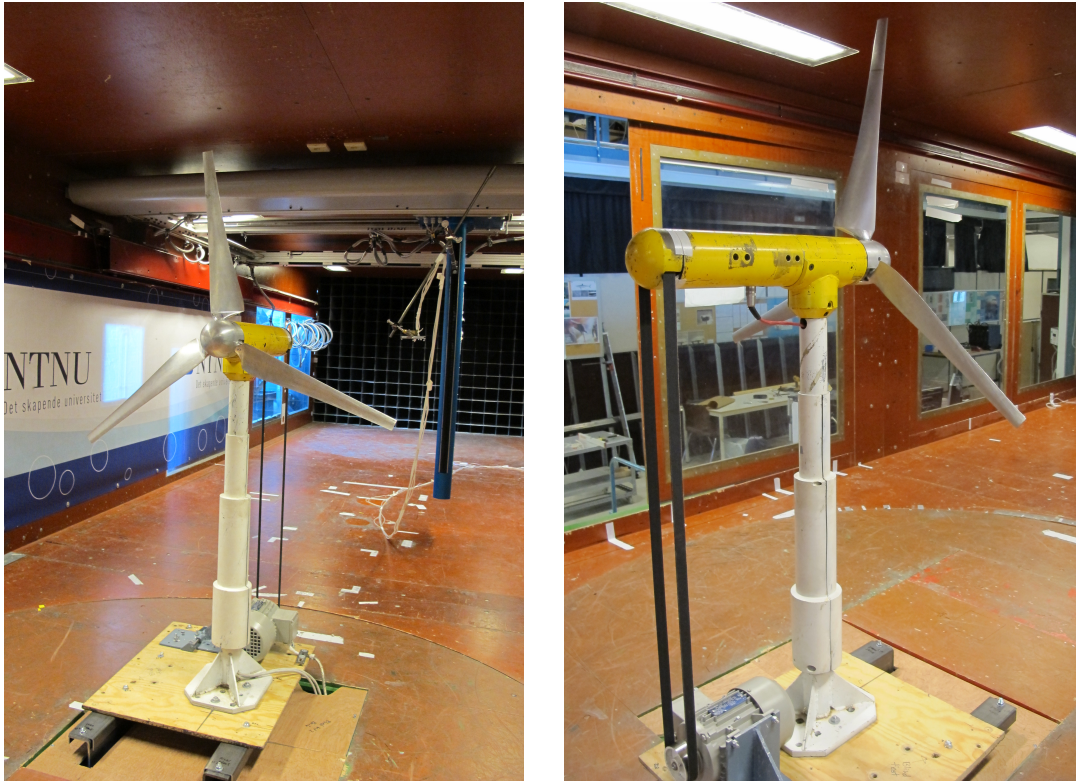
(a) Turbine from the front

(b) Turbine from the back

Figure 3.4: Scaled, Horizontal Axis Wind Turbine

3.1.2.1 Torque transducer

A HBM T20W $N/2Nm$, torque transducer is connected to the rotor shaft on the model turbine, measuring the torque produced by the turbine. When calibrating the torque transducer, a clamp was fastened at the end of the rotor shaft creating a torque at the front of the shaft. Weights of fixed sizes were attached to one of the turbine blades at a defined distance from the center of rotation. The weights generated a torque of defined values $[Nm]$. The measured values were related to volt signals $[V]$ in LAbVIEW, creating a linear relationship.

3.1.3 Instruments

In the experiments a five-hole pitot probe was used as measuring instrument, to evaluate the development of the wake. A thermocouple was used to measure the density during the experiments.

3.1.3.1   Five-hole pitot probe

A five-hole pitot probe makes it possible to measure the magnitude and direction of the velocity components in an unknown airflow. The head of the probe, used in this experiment, is shaped as a sphere and the five holes are distributed about the center of the head. By Bernoulli's equation a relationship between the pressure, measured in each hole, and the velocity distribution in the flow can be constructed [21]. The relationship between a position in the free stream and a point at the probe's head is determined by the following expression:

$$p - p_n = \tfrac{1}{2} \times \rho(U_n^2 - U^2) \qquad (3.5)$$

An advantage with a five-hole pitot probe is the possibility to measure angles of the velocity vectors. This makes it possible to evaluate the flow pattern with direction and magnitudes. The distribution of the five holes are illustrated in figure 3.5. The relationship between the yaw, ϕ, and roll, θ, angles and the velocity components are placed in a coordinate system in figure 3.6.
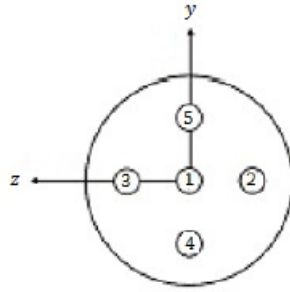

Figure 3.5: Distribution of the five holes on the surface of the five-hole pitot probe [11] (modified)
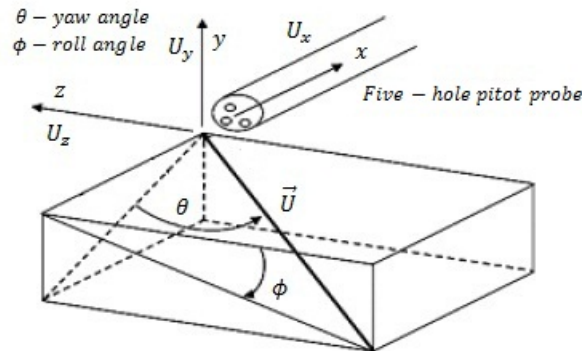

Figure 3.6: Five-hole pitot probe in coordinate system [11] (modified)

23

When the velocity vectors, $\overrightarrow{U}$, and the yaw and roll angles are identified, it is possible to find the velocity components in x, y and z direction by the following expressions:

$$U_x = U cos\theta cos\phi \hat{i} \tag{3.6}$$

$$U_y = U cos\theta sin\phi \hat{j} \tag{3.7}$$

$$U_z = U sin\theta \hat{k} \tag{3.8}$$

At the five-hole pitot probe used in this study, the pressure holes were not completely symmetrical distributed about the center hole. However, a comprehensive calibration technique, described below, corrected for asymmetries.

Calibration of the five-hole pitot probe   There are two procedures to accomplish measurements with a five-hole pitot probe: the nulling technique and the non-nulling technique. The nulling technique assumes a very accurate traverse system, where the probe is perfectly aligned with the flow in every measuring point [19]. This procedure requires a long time response and accuracy unobtainable for the purpose in this experimental study. Therefore the non-nulling technique was applied.

Schümann [27] performed the calibration for the five-hole pitot probe utilized in this experiment. A three dimensional curve-fit analysis program was developed in MATLAB for the calibration, using a modified routine of the approach presented by Morrison et al. [19]. The calibration was carried out in a circular test rig, with $0,185m$ in diameter and $14m$ in length. The velocity in the wind tunnel during calibration was $U = 8,8^m/_s$. The value was between the free stream velocity, U_∞, in the wind tunnel during the experiments and the expected lowest velocity in the wake [27]. The probe was mounted at the outlet of the wind tunnel and yaw and roll angles were traversed. From the measured results, non-dimensional calibration constants were developed. This was done to convert the pressure difference between the stagnation and static pressure to magnitude and direction of the velocity components in the flow (see equation 3.6, 3.7 and 3.8).

To reduce the effect of bad calibration points and the effect of the slightly asymmetric distribution of the pressure holes, a cubic interpolation was used between the data points.

3.1.3.2   Thermocouple

During the experiments, a thermocouple was mounted to the wind tunnel wall to record the temperatures in the tunnel. The registered values were used to calculate the air density in the wind tunnel by the relationship:

$$\rho = \frac{p_{atm}}{R_{spesific}T_{temp}} \tag{3.9}$$

Where p_{atm} is the atmospheric pressure, $R_{spesific}$ is the gas constant of air and T_{temp} is the measured temperature in the tunnel. The thermocouple was connected to the PC through a data-acquisition board and the temperatures were logged in LabVIEW.

3.1.3.3   Pressure Transducer

The five-hole pitot probe and the inlet contraction section were attached, with silicon tubes, to pressure transducers. The pressure transducer transformed the pressure signals, recorded in the flow, to volt signals $[V]$. The transducers were connected to a data-acquisition board which was attached to the PC. The signals were logged in LabVIEW. In all, seven pressure transducers were used in the experiment.

Calibration of the pressure transducers   During calibration, the pressure transducers were connected to a manually controlled manometer with silicon pipes. By adjusting the pressure in the pipes, using clamps, the height of alcohol in the alcohol column of the manometer and the volt signal logged in LabVIEW were varied. A relationship between the pressure, p, and the height of alcohol in the manometer, $h_{alcohol}$ $[m]$, is determined by:

$$p = h_{alcohol} \times g \times \rho \tag{3.10}$$

In the equation g represents the acceleration of gravity $[m/s^2]$ and ρ, the density of the alcohol $[kg/m^3]$. Methylated spirit with a density of $810 kg/m^3$ was applied in the manometer.

The pressure values were plotted against volt signals and a linear relationship was created. In figure 3.7 the calibration curve of one of the pressure transducers is shown.
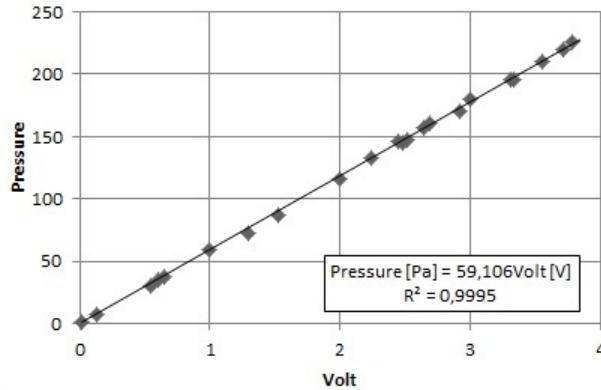
Figure 3.7: Calibration curve of pressure transducer

The offset values were slightly varied and the pressure constant was not persistent. Thus, it was necessary to calibrate the pressure transducers before every experiment.

3.2   Set-up

During the experiments the same arrangement of the measuring instrument was utilized. Measurements behind the turbine were performed with two different set-ups. The first experiments were performed with the original model turbine in the wind tunnel, while the other part of the experiments were performed with an additional tower mounted above the turbine.

3.2.1   Arrangement of measuring instruments

The set-up of the measuring instrument is shown in figure 3.8. The five-hole pitot probe was fastened with a steel arrangement, adjustable in several directions to make the probe in line with the flow at all time. The arrangement was mounted to the traverse system, which made it possible to take measurements over the entire cross-section.
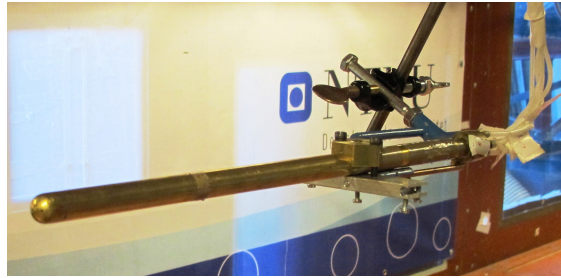
Figure 3.8: Arrangement of measuring instrument

3.2.2   Set-up: Single turbine in tunnel

The velocity profiles and the performance characteristics were measured by placing the turbine in the tunnel, with equal distance to the tunnel wall and with a distance of $4,5D$ to the entrance. The turbine was mounted to the force balance. The traverse, with the measuring arrangement, was moved to the desired distance behind the turbine and measurements were performed. The set-up is shown in figure 3.9.
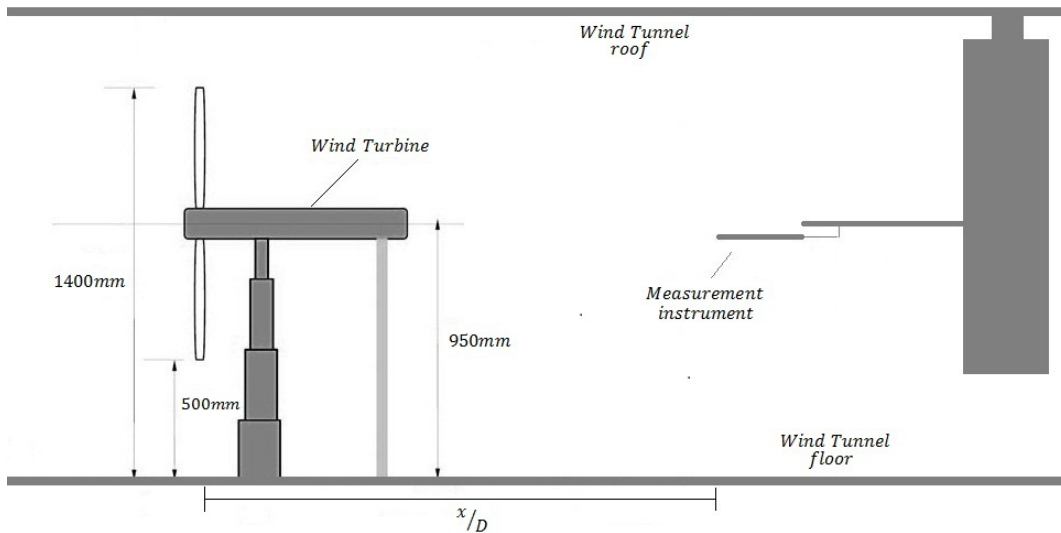
Figure 3.9: Model turbine in wind tunnel with measurement instrument

3.2.3 Set-up: Turbine with additional tower

To evaluate the influence of the tower, an additional cylinder equal to the tower of the turbine was mounted to the roof. The set-up is shown in figure 3.10. The additional cylinder was made of steel and wood. Close to the hub, a part of wood was added to be able to fit the supplementary tower to the hub. The distance between the hub and the tower was approximately $5mm$. The cylinder did not touch the hub because it was not desirable to influence the force balance with additional weight.

Figure 3.10: Turbine with additional tower

Chapter 4

Results and Discussion

4.1 Measurements behind turbine

Measurements were performed behind the turbine at different distances downstream. During the experiments the turbine was operating at zero pitch and yaw angles. First performance curves were obtained by collecting signals from the force balance and torque transducer, at different loads and rotational speeds. A five-hole pitot probe was used to measure the velocity components behind the turbine, to investigate the evolution throughout the wake. Measurements without tower were carried out at $0,5D$, $1D$, $1,5D$, $2D$ and $3D$ to investigate the development of the tower shadow. Measurements with the additional tower were performed at $0,5D$ and $3D$ behind the turbine to examine the influence of the tower on the wake by creating symmetry about the hub. During the experiments the free stream velocity was $11^{m}/_{s}$. In addition, it was desirable to examine the influence of the free stream velocity on the turbine behavior. The same measurements were therefore performed at a free stream velocity of $7,5^{m}/_{s}$, at $0,5D$ downstream of the turbine, both with and without the additional tower. The free stream velocity was monitored and kept constant throughout all the experiments by controlling the contraction velocity measured at the inlet section of the tunnel. In this chapter the results from the measurements will be presented.

4.1.1 Measurements behind single turbine

4.1.1.1 Characteristic curves

The performance of the turbine is the net energy output, non-dimensionalized over the available power from the free stream. During the energy extraction process, the wind applies a thrust force and a torque on the turbine rotor. The thrust force was measured by positioning the turbine on the force balance, while the torque was estimated by means of the torque transducer connected to the shaft of the turbine. By adjusting the rotational velocity of the turbine and measuring for every single working condition, the performance coefficients were obtained. In figure 4.1 the power coefficient, C_p, of the

turbine is presented against the Tip Speed Ratio, TSR, and in figure 4.2, the thrust coefficient, C_T, is presented.

While obtaining thrust and power coefficients, the contraction velocity of the wind tunnel was $U_\infty = 11^{m}/s$. Performance characteristics for the present turbine were previously investigated by Loland [15], Adaramola and Krogstad [1] and Bartl [5].

Analyzing figure 4.1, the results indicates that the turbine operated at optimal when the TSR value was $5, 5$ at the free stream velocity. The peak power coefficient turned out to be 0.45. Here the turbine operated at ideal conditions. The curve developed as expected from the theoretical results, described in chapter 2.3. The power coefficient increased until it reached a maximum value at $5, 5$. With further increase in TSR, the power coefficient decreased, as anticipated. The experiment should contain some more points at higher TSR values, to include the maximum TSR value where power could be extracted. This was not feasible because of technical problems which arose during the experiment.
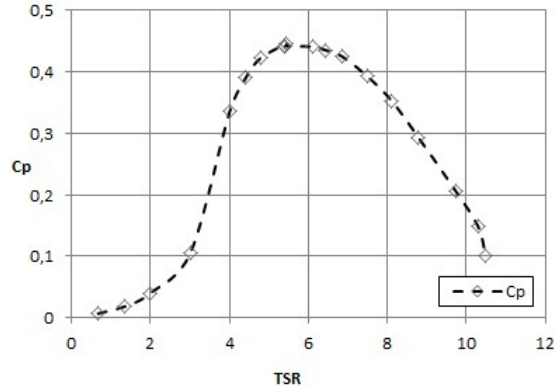
Figure 4.1: Power coefficient

Adaramola and Krogstad [1] performed a comprehensive study of the performance characteristics and near wake of the same turbine as the present experiment, in yawed conditions. The experiment was performed in the same wind tunnel at a free stream velocity of about $10^{m}/s$. The maximum power coefficient in their experiment was found to be $C_p = 0, 45$, when the turbine was operating at zero pitch and yaw angles. The corresponding Tip Speed Ratio at this point was $TSR = 6$. In this experiment the 'runaway TSR' was about $11, 2$ [1]. Bartl [5], performed a similar experiment with the same equipment's. At an inflow speed of $U_\infty = 11, 5^{m}/s$, a power coefficient of $0, 47$ was obtained. The highest TSR value achieved, during the experiment, was $11, 6$ [5]. From the tendency which can be extrapolated from the last acquired points, it can be inferred that the runaway point of the present experiment was located somewhere between $11, 2$ and $11, 6$. The structure of the curve and values obtained in figure 4.1, were in agreement with the results acquired by [1, 5, 15].

The thrust coefficient is presented in figure 4.2 below. To calculate the thrust

induced by the rotor, the thrust of the tower and nacelle had to be subtracted from the total measured drag force. For this reason, measurements were performed on the tower and the nacelle when the blades were taken off.
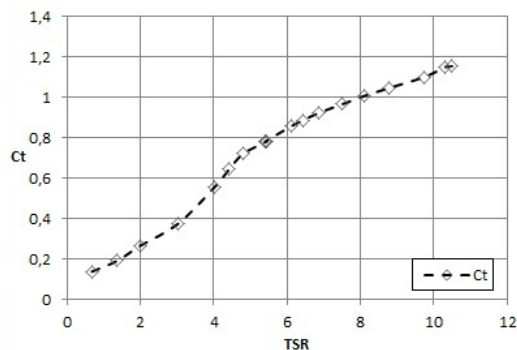
Figure 4.2: Thrust coefficient

With growing TSR, the rotational speed got higher. The disc became more "solid" and the thrust force acting on the turbine increased. The maximum thrust coefficient was obtained at $1, 15$. This occurred at a TSR value of $10, 3$. Between approximately $TSR = 3$ and $TSR = 5, 5$ there was a steeper increase in the C_T curve. This was due to the transition from the stalled region to optimal operation, also experienced in the development of the C_p curve. At $5, 5$ the turbine was no longer working under stalled conditions. The value of the C_T measurements exceeded one. This was probably due to the blockage effect from the wind tunnel walls, contributing to increase the local velocity which resulted in a higher thrust force acting on the turbine. Compared to the experiments previously mentioned, [1] and [5], it was expected that the C_T value would reach $1, 2$ at higher TSR values. Due to technical problems, measurements in this region were not performed.

However, the results coincide with the results recorded by [1, 5, 15].

4.1.1.2   Wake development

In figure 4.3, the mean velocity distribution is shown for $0, 5D$, $1D$, $2D$ and $3D$ downstream of the turbine. The values are non-dimensionalized over the free stream velocity U_m/U_∞. The measurements were taken horizontal over the cross-section of the tunnel, at hub height. During the experiments the turbine was operating at optimal conditions at $TSR = 5, 5$.
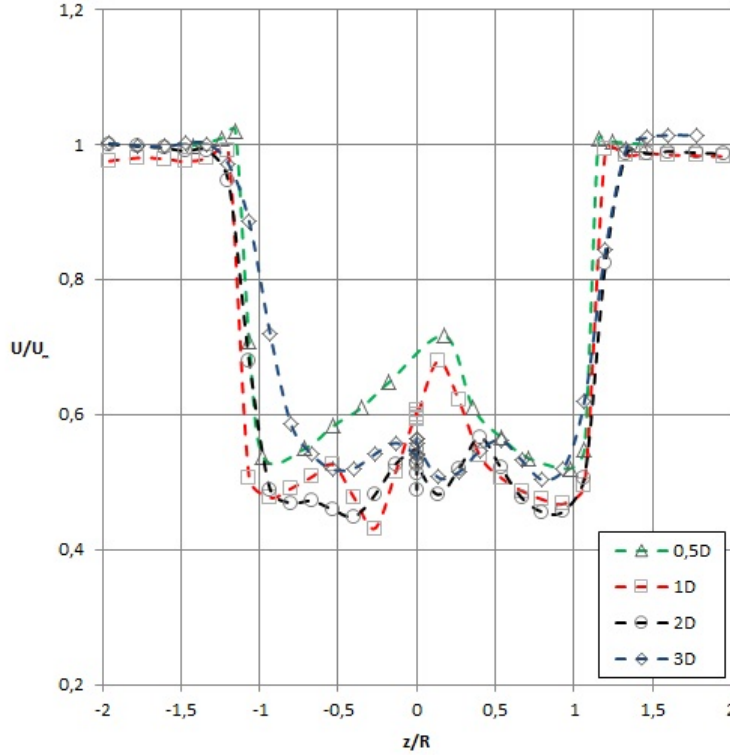
Figure 4.3: Axial velocity profile at 0,5D, 1D, 2D and 3D

As expected, a deep velocity deficit was present, in agreement with theory presented in chapter 2.5. At $0,5D$ and $1D$ downstream of the turbine the profiles were characterized by considerable variations in the middle of the wake. The close distance to the hub and tower contributed to these irregularities in the wake development. Strong root vortices also caused the asymmetric behavior in this area. At $0,5D$ the lowest velocity was $U_m/U_\infty = 0,54$ and at $1D$ the lowest velocity was measured $U_m/U_\infty = 0,43$. Further downstream, the profile got flatter and the velocity deficit was reduced. At $2D$ downstream the minimum velocity was $U_m/U_\infty = 0,45$ and at $3D$ $U_m/U_\infty = 0,5$.

The velocity $0,5D$ downstream from the rotor was averagely higher than the velocity at $1D$, as expected from the actuator disc theory (see figure 2.1). The velocity decreased gradually as the pressure drop recovered and increased again because of the turbulent mixing and wake expansion.

As the wake propagated downstream the wake width increased. The turbulence in the wake mixed the lower velocities in the wake with the higher velocities in the free stream. At $0,5D$ the width of the wake was $\triangle(z/R) = 2,3$. At $3D$ downstream, the wake expanded to $\triangle(z/R) = 2,6$. At close distance behind the turbine, influence from the tip vortices created a sharp velocity gradient between the wake and the free stream, $z/R = \pm1,16$, at $0,5D$. At $2D$ and $3D$ the transition was smoother because the turbulent diffusion smeared out the velocity gradients further behind the turbine. As a result the wake became broader and the velocity deficit decreased.

Movement of tower shadow   Figure 4.4 shows full area profiles of the mean velocity of the wake development, at different distances downstream of the turbine. The profiles are non-dimensionalized by the free stream velocity, U_m/U_∞.
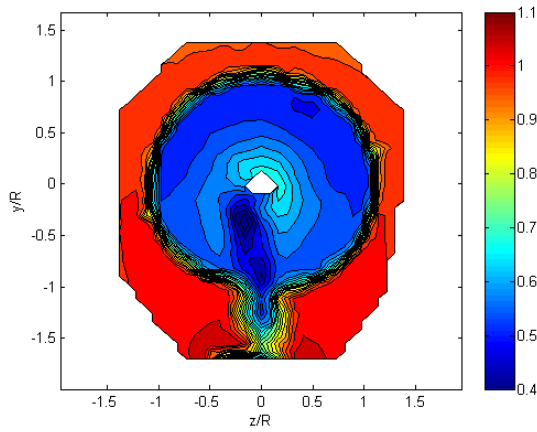
(a) 0,5D
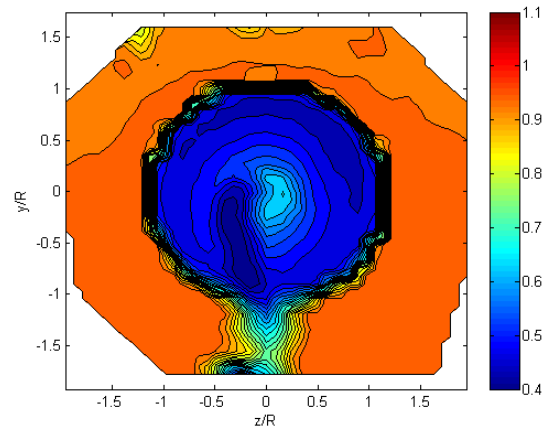
(b) 1D
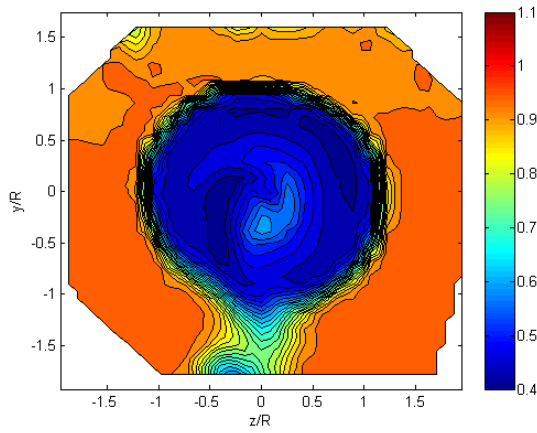
(c) 1,5D
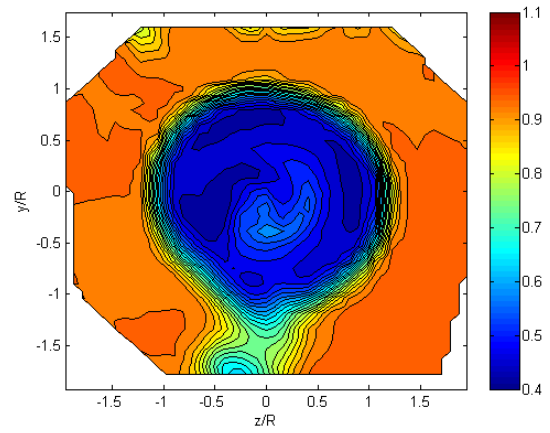
(d) 2D
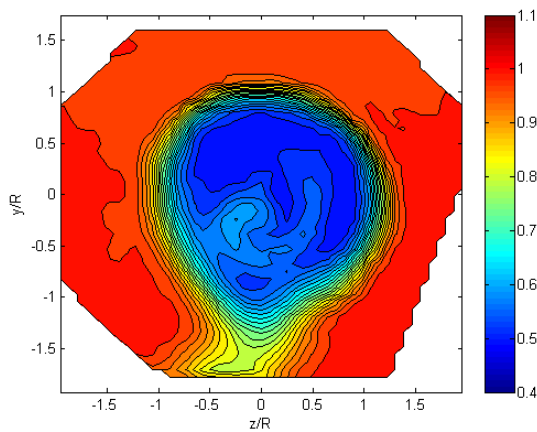
(e) 3D

Figure 4.4: Full area velocity profiles at $0,5D$, $1D$, $1,5D$, $2D$ and $3D$

Figure 4.4a shows the mean velocity profile $0,5D$ downstream from the turbine rotor. The tower shadow was clearly visible to the left of the center of rotation, as a region of lower velocities than the surrounding flow. In the middle of the figure there was an open region where no valid measurements were available: here the five-hole pitot probe was not able to capture the different components of the flow due to the presence of the nacelle, which induced backflow and other disturbances. In figure 4.4b and figure 4.4c the tower shadow was still evident, drifting in clockwise direction as the wake propagated further downstream. At $2D$ downstream (see figure 4.4d), the outline of the tower was less pronounced, but present at a nine o'clock position. At $3D$ downstream (see figure 4.4e), the tower shadow merged with the surrounding airflow. Barber et al. [4] investigated the wake behind a single turbine using a five-hole pitot probe. Their measurements discovered a: "significant asymmetry caused by the tower, as the surrounding flow migrates into the lower-pressure region of the tower's wake" [4]. Kress et al. [12] also discovered asymmetries due to the presence of the tower. Nygard [22] investigated the influence of the tower wake on the rotor wake, at different operating conditions. He observed that: "As the wake propagates downstream the tower wake is displaced due to a clockwise rotation of the wake" [22]. This is in accordance with the results found in figure 4.4.

Due to the presence of the nacelle the energy extraction was lower in the area behind the hub, contributing to a region of higher velocities. In figure 4.4a the area of higher velocity was located behind the rotor center, creating a velocity difference between the inner and outer part of the wake. At the center the velocity was theoretically zero. Moving downstream the higher velocity region relocated, influencing the movement of the tower shadow as well. The tower wake rotated faster at the center and slower at the outer part of the wake. In figure 4.4e the area of higher velocities had drifted down and to the left of the origin. Barber et al. [4] noticed a similar development in their study.

Close to the top of figure 4.4b, 4.4c and 4.4d an area of lower velocities was visible. These disturbances were probably due to the presence of the traverse system and the close distance to the roof. The traverse system was mounted to the tunnel roof creating a blockage effect in this area that influenced the free stream velocity. Observing the overall wake development in figure 4.4 it was clear that the wake expanded more in the horizontal direction than in the vertical direction. Referring to figure 4.3, the wake expanded, at $3D$, from $z/R = -1,3$ to $z/R = 1,3$ in horizontal direction, while in vertical direction it only grew to $y/R = 1,2$ above the rotor axis. Bartl [5] and Adaramola and Krogstad [2] also experienced influence from the roof in their experiments, since the hub was located only $1,1D$ below the roof.

Development of rotation   The Arrows in figure 4.5, are velocity vectors projected on the cross-sectional plan y-z, at $0,5D$ and $3D$ downstream of the turbine. The wake rotates in clockwise direction. In figure 4.5a the arrows revolve about the origin at $0,5D$.

Further downstream, the rotational axis seemed to move. At $3D$ (see figure 4.5b) the center of rotation moved approximately $y/R = -0,25$ and $z/R = -0,1$. A dislocation of the rotation was also evident in figure 4.4 where the area of higher velocities moved, as previously described.
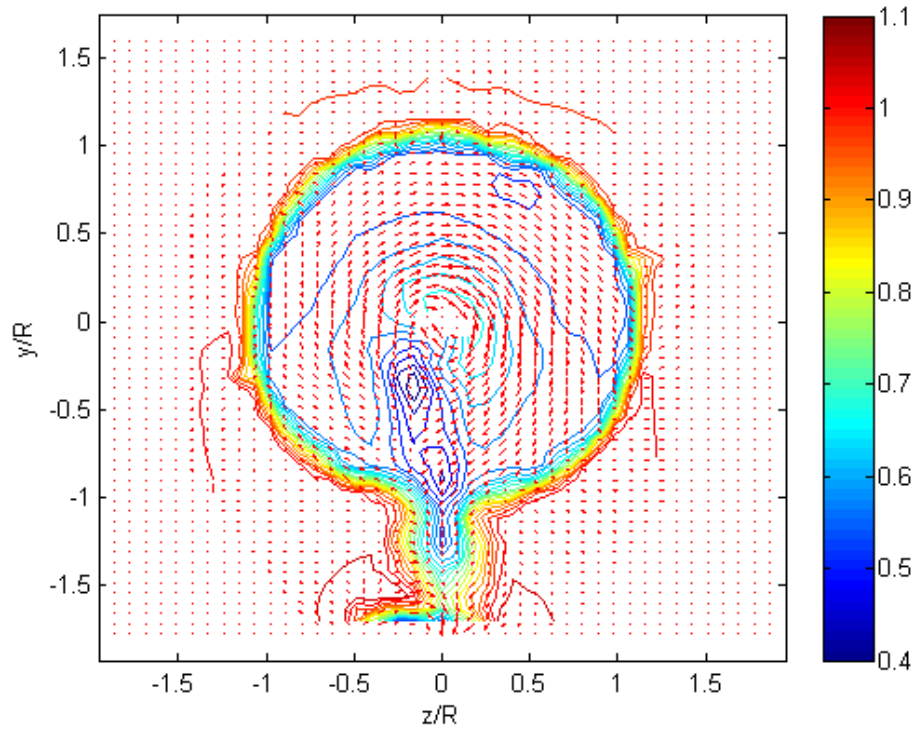
(a) 0,5D
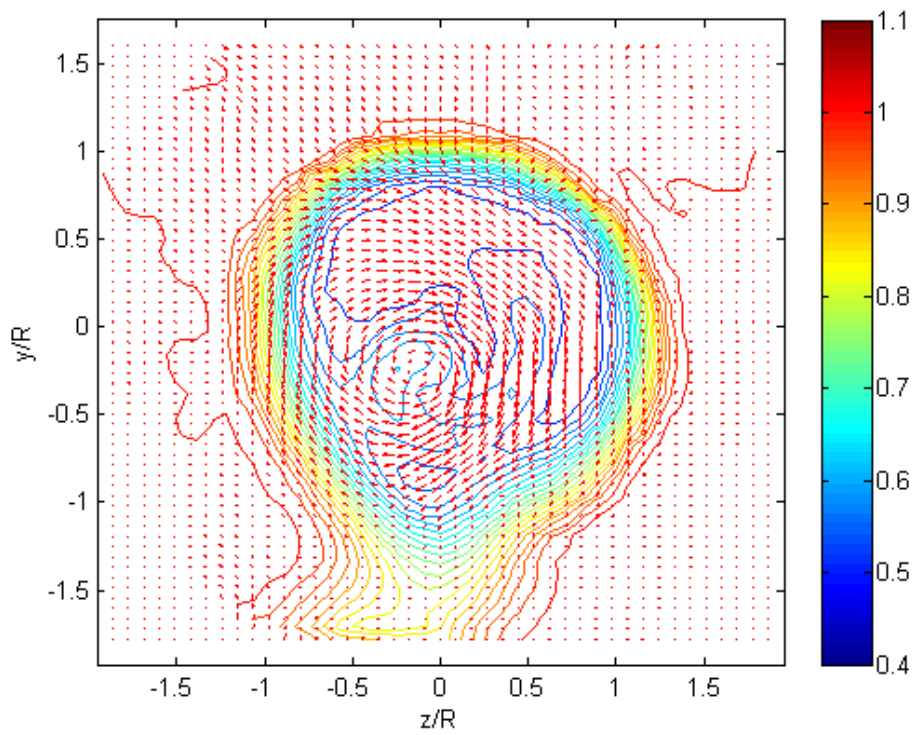
(b) 3D

Figure 4.5: Vectorial velocity components at 0,5D and 3D

36

Previous studies [5, 6, 9, 23, 28, 29, 16] also highlighted a certain downshift of the rotational axis. Blomhoff [6], Eriksen [9] and Pierella [23] performed their experiments in the same wind tunnel, behind the same turbine as the present study, under similar conditions. Maeda et al. [16] investigated the interaction between two turbines under different flow patterns. The study discovered that: "The axial velocity distribution is distorted, and a weak velocity area appears below the center of the rotor axis" [16]. The paper suggested that the reason for the displacement could be the influence of the tower wake. Bartl [5] also assumed that a lower pressure region behind the tower could cause the experienced downshift. Talmon [28, 29] investigated the effect of the tower, the nacelle and the ground, on the wake. The experiment showed a certain downshift of the velocity deficit [30]. These findings were further examined by Crespo et al. [8] who ascribed the results to the effect of the ground and the shear of the incoming flow [30]. However, the turbine hub was centered closer to the roof than to the floor in the present experiment. Consequently, if the tunnel walls were responsible for the downshift, the rotational axis should have shifted upwards. Accordingly, the presence of the ground was unlikely to be the reason for the downshift experienced in this study. Furthermore, Bartl [5], who performed a similar experiment in the same wind tunnel as the present study, stated that: "there is no shear in the inlet flow field" [5]. Thus, the shear could not be the reason for the downshift of the rotational axis.

Figure 4.6 shows the development of the tangential velocity components at $0, 5D$ and $3D$ downstream of the turbine. The measurements were taken across the cross-section, at hub height.
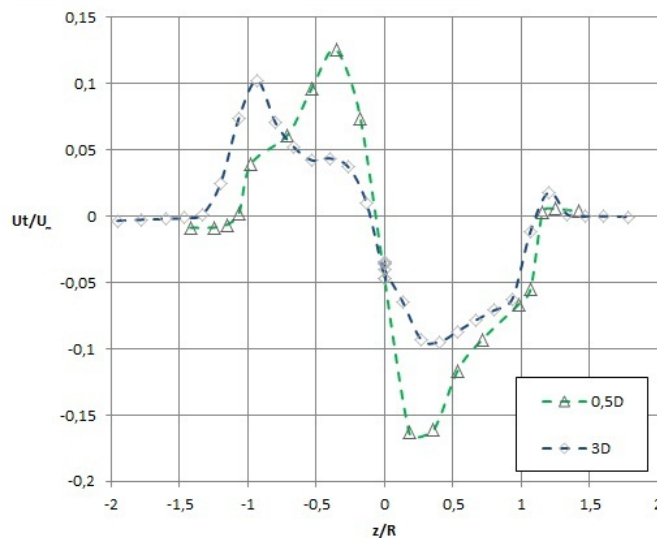
Figure 4.6: Tangential velocity profile at $0, 5D$ and $3D$

At $0, 5D$ the components had a maximum value at $z/R = -0, 36$ and $z/R = 0, 36$, the corresponding tangential velocities in these points were $|U_t/U_\infty| = 0, 13$ and $|U_t/U_\infty| = 0, 16$. Compared to figure 4.5a, the rotation was located near the origin and the devel-

opment was expected to be close to symmetric through the wake. At $3D$ the profile was less symmetric and the tangential components were clearly reduced. Here the maximum velocities at each side of the axis were found at $z/R = -0,93$ and $z/R = 0,27$ with values of $|U_t/U_\infty| = 0,1$ and $|U_t/U_\infty| = 0,09$. The wake moved to the left of the origin, with zero tangential velocity components at approximately $z/R = -0,1$. This result was in accordance with the information found in figure 4.5b. The strong tangential components at approximately $z/R = -1$ could also be seen at the almost vertical arrows in figure 4.5b.

4.1.2   Measurements behind turbine with additional tower

Measurements with additional tower, as described in chapter 3.2.3, were performed at $0,5D$ and $3D$ downstream of the turbine. In figure 4.7 the mean velocity distribution is shown, U_m/U_∞.

(a) 0,5D   (b) 3D
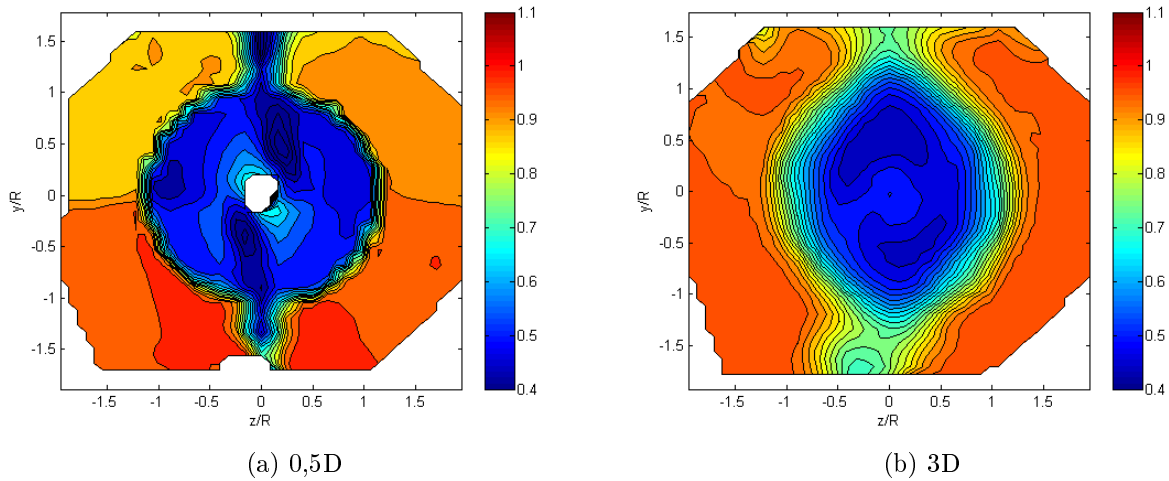
Figure 4.7: Full area velocity profiles with additional tower at $0,5D$ and $3D$

The shadow of the additional tower was clearly visible at $0,5D$ (see figure 4.7a). The wake was well defined at close distance behind the turbine, with an abrupt transition to the free stream with higher velocities. The tip vortices were clearly visible in the transition area, under form of a steep velocity gradient. Moving downstream the outline of the wake became more diffuse (see figure 4.7b). The lower velocities in the wake mixed with the higher velocities in the free stream, resulting in expansion and a broader wake. At $0,5D$ the velocity right behind the hub was not captured, as it had happened in the measurements without additional tower. The velocity components were outside the interval of the calibration area of the five-hole pitot probe, and the results were not reported. At $3D$ the profile was more uniform over the cross-section compared to the case without an extra tower (see figure 4.4e).

At $0,5D$ the area of higher velocities, also registered in the measurements without the additional tower (see chapter 4.1.1.2), due to the presence of the nacelle, was still present. At $3D$ this contribution was still evident, albeit less visible, right on the origin.

In figure 4.8 transversal velocity vectors describe the rotation of the flow at $0,5D$ and $3D$ downstream of the turbine, with additional tower.
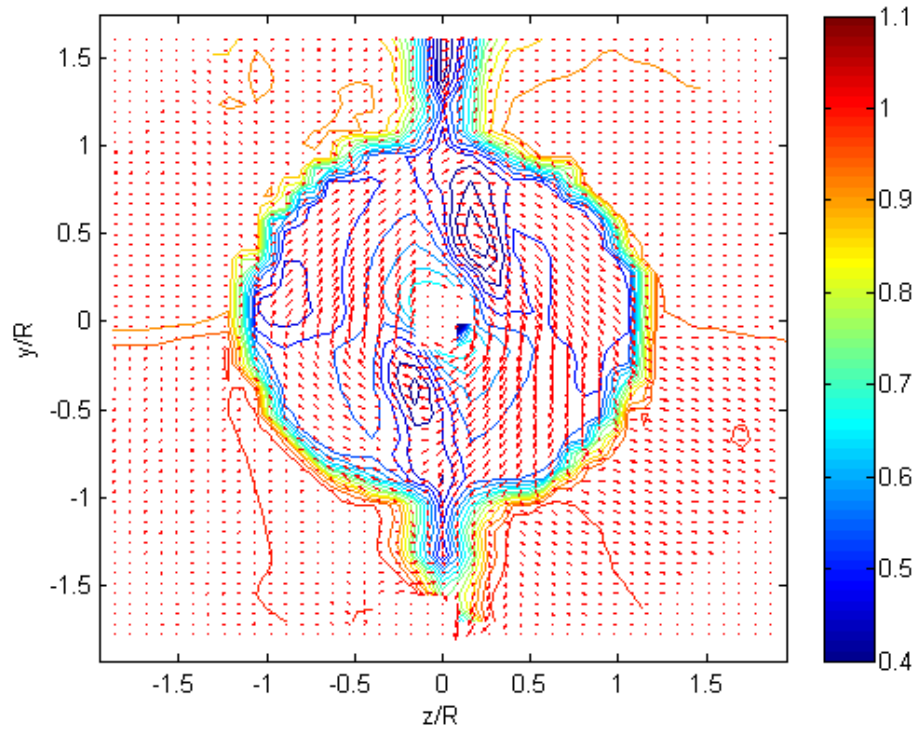
(a) 0,5D
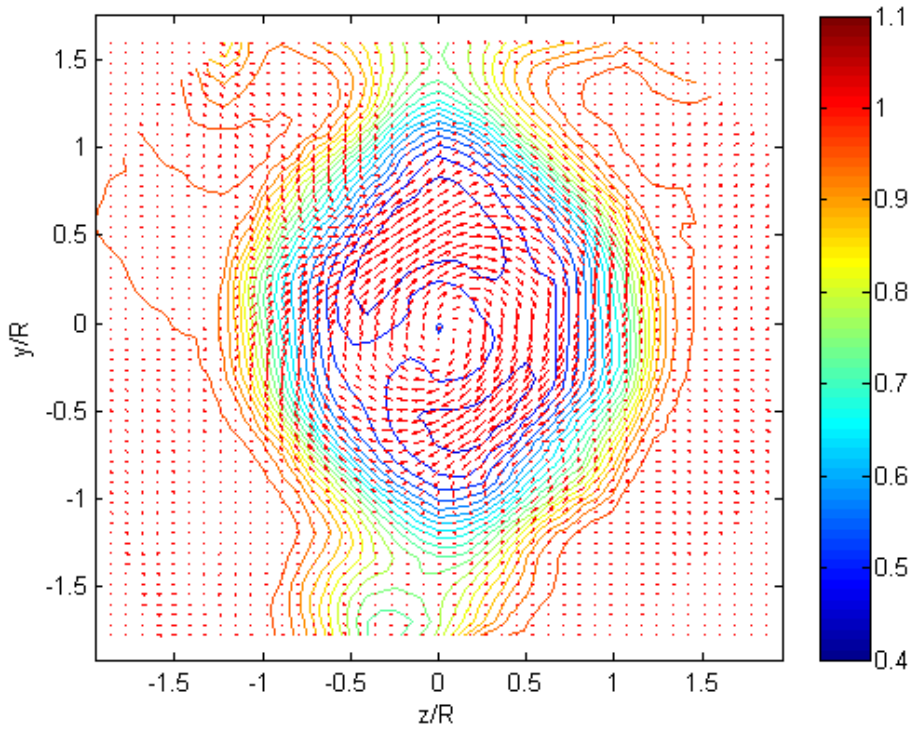
(b) 3D

Figure 4.8: Vectorial velocity components with additional tower at $0,5D$ and $3D$

At 0,5D downstream from the rotor, comparing figure 4.8a to figure 4.5a, the rotation with additional tower did not deviate strongly from the case without tower. The rotation shown in figure 4.8a was close to symmetric across the wake. At $3D$ the additional tower contributed to the development of the wake. In figure 4.5b the center of rotation was significantly shifted down. With the additional tower (see figure 4.8b), the center of rotation was located right at the origin and the rotation was close to symmetric about the axes.

In figure 4.9 and 4.10 the axial and tangential velocity profiles with additional tower, at $0,5D$ and $3D$, are shown.
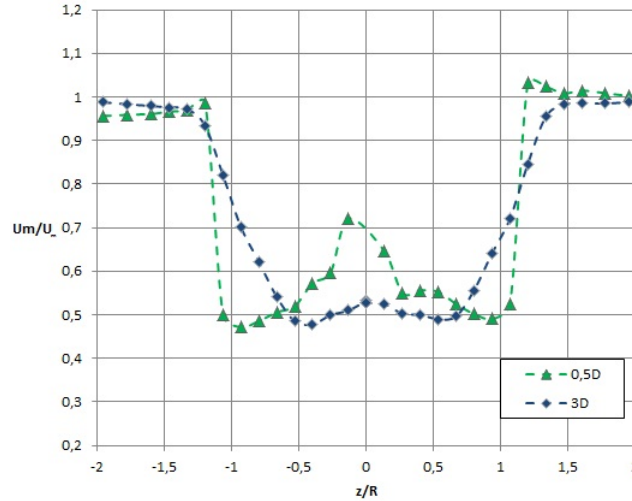
Figure 4.9: Axial velocity profile with addditional tower at $0,5D$ and $3D$

At $0,5D$ the profile was dominated by disturbances in the middle of the wake. Here contribution from the towers and the presence of the hub, as well as root vortices, influenced the development of the wake. This was also noticeable in figure 4.3 at close distance from the turbine. However, the disturbances evened out further downstream and were less visible $3D$ downstream. The velocity deficit gradually recovered at increasing distance from the rotor. At $0,5D$ the lowest velocity was found at $z/R = -0,93$. Here the velocity in axial direction was $U_m/U_\infty = 0,47$. At $3D$ the velocity minimum increased to $U_m/U_\infty = 0,48$ at $z/R = -0,4$.

Moving downstream the wake expanded from $\triangle z/R = 2,4$ at $0,5D$ to $\triangle z/R = 2,8$ at $3D$. This was slightly broader than the measurements without the additional tower.
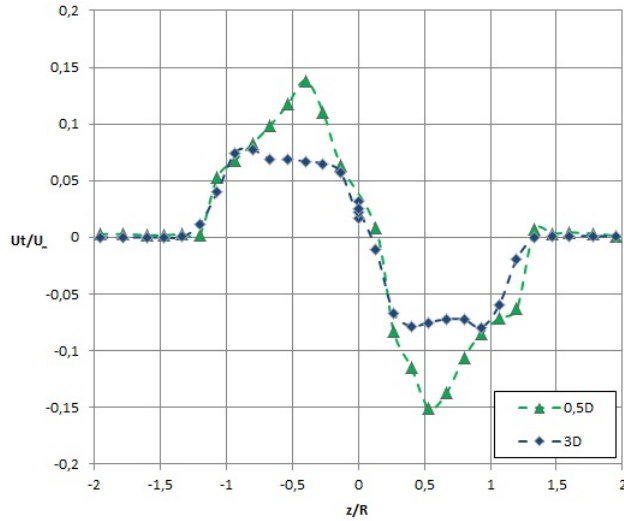
Figure 4.10: Tangential velocity profile with additional tower at $0,5D$ and $3D$

The tangential distribution is shown in figure 4.10. At $0,5D$ the maximum velocities were found at $z/R = -0,4$ and $z/R = 0,53$. The corresponding tangential velocities were approximately $|U_t/U_\infty| = 0,14$ and $|U_t/U_\infty| = 0,15$. Zero velocity was found slightly to the right of the origin. Moving downstream, the profile was almost symmetric. The maximum tangential velocity, 3D behind the turbine, was found at $z/R = \pm 0,9$, the velocity in these points was $|U_t/U_\infty| = 0,09$. In both cases the point of zero velocity was found at $z/R = 0,1$.

4.1.3 Comparison with and without tower

Comparing measurements with and without the additional tower it was clear that the tower influenced the experienced downshift. Figure 4.5b showed a significant downshift of the rotational axis. Adding the extra tower, creating similarity about the hub, the downshift was no longer noticeable (see figure 4.8b).

In figure 4.11 the axial and tangential velocity profiles, at hub height, $0,5D$ and $3D$ downstream of the turbine, both with and without the additional tower, are plotted against each other.

(a) 0,5D - axial velocity distribution

(b) 3D - axial velocity distribution

(c) 0,5D - tangential velocity distribution

(d) 3D - tangential velocity distribution
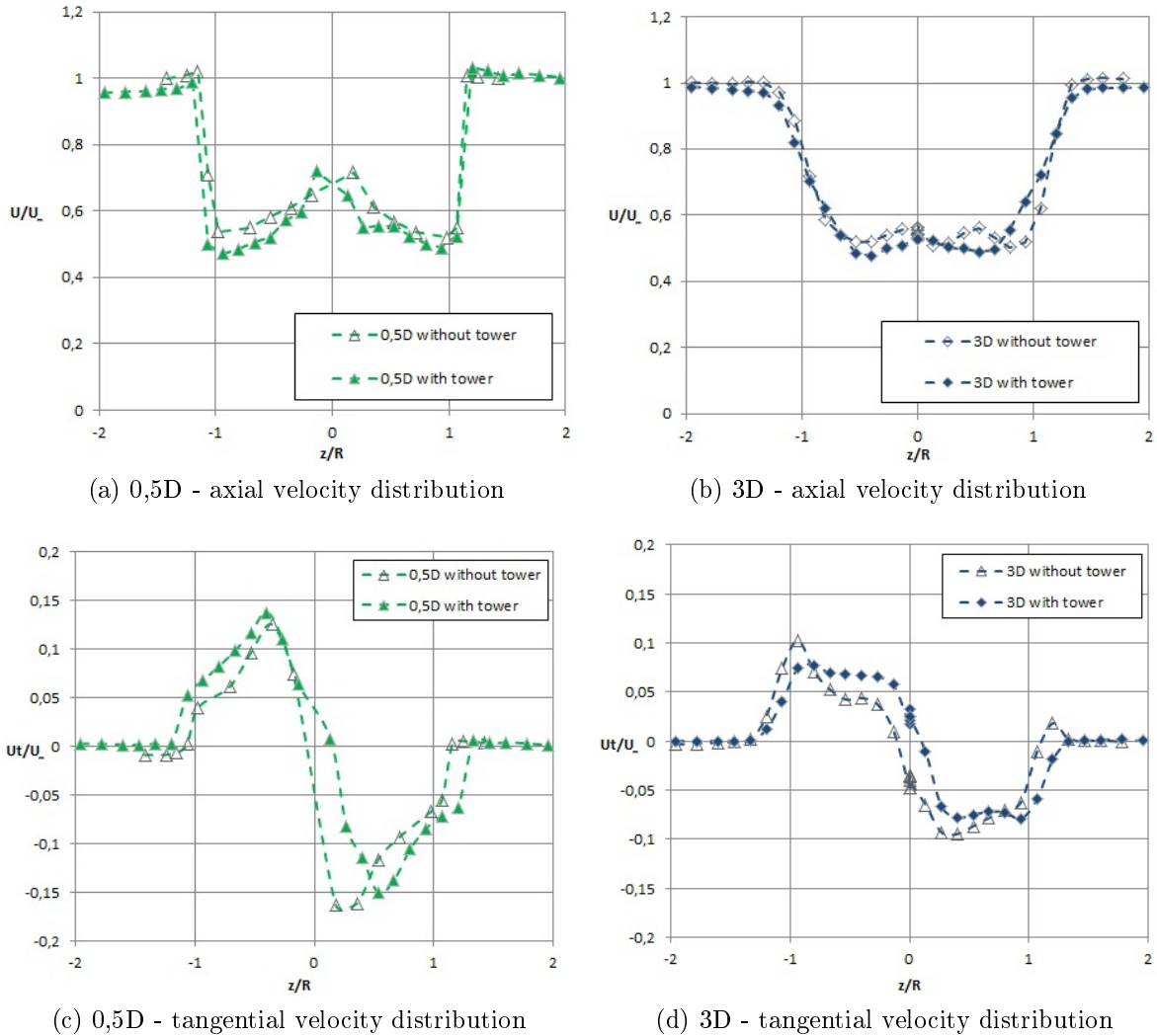
Figure 4.11: Axial and tangential development with and without tower at $0,5D$ and $3D$

The velocity deficit in figure 4.11a and 4.11b was in both cases larger with the additional tower mounted above the turbine. This is because the extra tower created supplementary resistance in the tunnel. At the same inlet velocity, this turned out in lower non-dimensionalized axial velocity in the case with an additional tower. At 0,5D both with and without tower, the central part of the wake was characterized by disturbances. As previously mentioned this was due to the close distance to the hub, creating a non-uniform profile across the wake. $3D$ downstream of the turbine (see figure 4.11b) the profiles were more constant through the wake. The plot of the velocity with the additional tower, had almost no disturbances in the center of the wake and the profile was close to symmetric about the origin. Without the tower the profile had more disturbances and was less symmetric.

43

The wake with additional tower was slightly broader than the measurements without additional tower. This could possibly be because the supplementary tower generated extra turbulence, which contributed to an increased wake and to an increased momentum loss.

Figure 4.11c and 4.11d shows the tangential velocity distribution at 0,5D and 3D downstream of the turbine. The somewhat asymmetric development at 0,5D could be ascribed the close distance to the nacelle and influence from the tower, also noticeable in figure 4.9. However, at 3D downstream of the turbine the profile was almost symmetric across the wake with the additional tower. Both at 0,5D and 3D the profiles were oriented slightly to the right of the origin, compared to the measurements without tower, where the profiles shifted more to the left. Overall the tangential distribution seemed more symmetric with the additional tower compared to measurements without the tower.

The symmetric development of the flow with the additional tower, makes it adequate to assume that the tower was the reason for the experienced downshift of the rotational axis.

4.1.4 Measurements at lower velocities

To investigate if the movement of the tower shadow would be influenced by a lower free stream velocity, the contraction velocity was set to $7.5^{m}/_{s}$. It was desirable to let the turbine operate at optimal conditions, so the rotational speed was adjusted. Figure 4.12 shows the measurements at $0,5D$ downstream of the turbine, figure 4.12a without tower and figure 4.12b with additional tower.

(a) 0,5D without tower

(b) 0,5D with tower
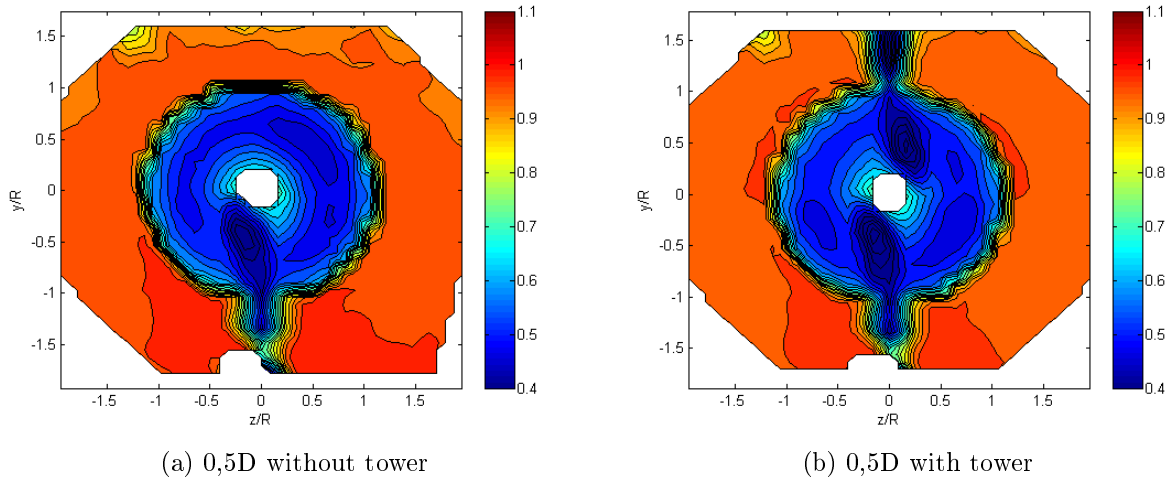
Figure 4.12: Full area velocity profiles at $U_\infty = 7,5^{m}/s$ without and with additional tower at $0,5D$ and $3D$

44

Compared to figure 4.4a and figure 4.7a the tower shadow did not moved noticeably different with a lower wind speed. Here as well, the measurements were not able to capture the components in the center of the wake. Analyzing figure 4.12 the velocity across the cross-section was less uniform than with a higher free stream velocity. With a free stream velocity of $U_\infty = 11^{m/s}$ the velocity distribution was almost constant across the blade. Working at optimal conditions the greatest amount of energy could be extracted. Krogstad and Lund [14] performed a Reynolds independent test on the same turbine in the same wind tunnel as the present study. According to their study: "It was found that the power coefficient curves were virtually independent of velocity for $U_\infty \geq 9^{m/s}$" [14]. This indicates that the turbine was operating in a Reynolds dependent area in the present study, with a free stream velocity of $U_\infty = 7,5^{m/s}$. The velocity distribution across the blades was non-uniform and less energy was extracted, because the blades did not work under optimal conditions. However, measurements could be taken further downstream to investigate if the tower shadow would move differently at other positions behind the turbine.

4.2 Measurement Uncertanties

There are several sources of uncertainties influencing the accuracy of the measurements during an experiment. American Society of Mechanical Engineers, ASME [3], suggests five classes to arrange these uncertainties: "Calibration uncertainties, data-acquisition uncertainties, data-reduction uncertainties, uncertainties due to methods and other uncertainties" [32].

Calibration of the measurement instruments is performed to minimize the uncertainty and to increase the reliability of the instruments. Nevertheless, some deviation will occur due to uncertainties in standards, uncertainties in the calibration process and other randomness [32]. During the calibration of the pressure transducers, the instruments were connected to a manually controlled manometer where the height of the alcohol column was read. The height of the column was not entirely constant and some deviation may influence the results. To minimize the errors, several points were taken when calibrating the pressure transducers.

Through the process of data-acquisition, errors arise due to uncertainties when a specific measurement is made. When collecting the velocity components behind the turbine, mean values were registered. In each measurement 450 points were measured at $30Hz$ through 15 seconds. This was assumed to be sufficient enough, but an increased number of points could reduce the error. A mean velocity for each point was registered by:

$$U_m = \frac{1}{N}\sum U_i \tag{4.1}$$

45

The data varied about this value and was therefore a source of uncertainties. In each point, a *rms* - 'root mean square' value was registered. This corresponds to the deviation in each point [31]. With these measured values a confidence interval can be constructed.

While acquiring velocity components calibration curves where obtained, assuming a linear relation between volt signals recorded by the pressure transducers and the heights read from the alcohol column at the manually controlled manometer. Nonlinearity in the measurements could cause a source of data-reduction uncertainties.

Uncertainties due to methods are uncertainties attached to the techniques or methods applied in the process. An example is if the five-hole pitot probe was not properly aligned with the flow. If the angle was too large, the results would get inaccurate. However, during experimentation, a lot of effort were put into aligning the instrument with the flow. Furthermore, while calibrating the five-hole pitot probe, a refined calibration technique was applied to reduce the effect of bad calibration points [19] (see chapter 3.1.3.1). Another source of uncertainties to the methods applied, is due to spatial effects. During the experiments the temperature and the atmospheric pressure varied. To reduce this influence on the measurements, atmospheric pressure was read every day and the temperature was logged at each measurement point. A thermocouple was utilized to log the temperature in the wind tunnel. If the temperature at the wall was lower than the air temperature in the tunnel, due to thermal radiation, the thermocouple would read too low values and errors could arise [32].

Other sources of uncertainties might occur because of uncontrolled variables in the measurement process and absence of repeatability in the output of the measuring system [32].

In Appendix A an analysis of the uncertainties in the measurements is attached.

Chapter 5

Conclusion and Future work

5.1 Conclusion

Through this experimental study, wind tunnel experiments were performed to investigate the wake behind a scaled; Horizontal Axis Wind Turbine (HAWT). The measurements were performed to examine the experienced downshift of the rotational axis and the development of the tower shadow.

Characteristic curves   The performance tests of the turbine showed that the turbine efficiency had a peak at $TSR = 5, 5$. The maximum power coefficient at this point was $C_p = 0, 45$. The runaway TSR value was not measured due to technical problems which arose during the experiment, but was expected to be between $11, 2$ and $11, 6$. The thrust coefficient exhibited a monotone behavior and the highest measured C_T value was $1, 15$, achieved for a TSR of $10, 3$.

Wake development   Comparing the axial distribution at several distances behind the turbine, the wake developed as expected. A slightly higher velocity deficit was discovered at $0, 5D$, compared to the profiles further downstream. The velocity decreased gradually before the deficit started to recover. The lowest measured mean, non-dimensionalized velocity at $0, 5D$ was $U_m/U_\infty = 0, 54$ and at $1D$ the value was $U_m/U_\infty = 0, 43$. At $3D$ the velocity increased to $U_m/U_\infty = 0, 5$. At close distance behind the turbine, the middle of the profiles were dominated by disturbances ascribed the presence of the nacelle and tower. At greater distances from the turbine the disturbances evened out.

The tangential velocity components were reduced downstream of the turbine and the point of zero velocity drifted to the left of the origin.

Propagating downstream of the turbine the wake expanded in horizontal direction, as the turbulence in the wake mixed the lower velocities with the higher velocities in the free stream. Between $0, 5D$ and $3D$ the wake expanded from $\triangle(z/R) = 2, 3$ to $\triangle(z/R) = 2, 6$.

Movement of tower shadow   Evaluating the development of the wake, the contribution from the tower shadow was examined. Downstream of the turbine the wake rotated in clockwise direction. The lower pressure region behind the tower followed the wake movements, with a lower velocity than the prevailing wake. Due to a lower energy extraction behind the nacelle the velocity in this area was slightly higher than in the remaining part of the wake. Thus, the velocity distribution across the wake was not homogenous. Consequently the tower shadow moved faster at the center of rotation than at the outer part of the wake, creating an asymmetric velocity distribution across the wake. Moving downstream from the turbine the influence of the tower became less pronounced. At $3D$ the outline of the tower shadow was no longer noticeable.

Due to the close distance to the roof and the presence of the traverse system, a blockage effect prevented the wake to expand equally in horizontal and vertical direction. In horizontal direction the wake expanded to $z/R = \pm 1,3$, while in vertical direction it only grew to $y/R = 1,2$.

Development of rotation   Measurements at different distances downstream of the turbine showed a relocation of the rotational axis. At $3D$ downstream of the turbine the rotation moved approximately $y/R = -0,25$ and $z/R = -0,1$, to the left of the origin.

Measurements with additional tower   The same measurements were accomplished modified with an additional tower, creating symmetry about the hub. Analyzing the results it can be concluded that the tower was responsible for the experienced downshift. The rotational axis was no longer rifting with the tower shadow, but was centered about the origin. The development of the axial and tangential velocity components behaved more symmetric about the origin than the profiles without the additional tower. However, at close distance behind the turbine the profile was still dominated by disturbances in the middle of the wake, caused by the presence of the tower and the hub as well as root vortices.

The wake with an additional tower expanded more than the wake without the extra tower, from $\triangle(z/R) = 2,4$ to $\triangle(z/R) = 2,8$. Due to the extra tower supplementary turbulence was generated, resulting in increased wake expansion and increased momentum loss.

Measurements at lower velocities   At a free stream velocity of $7,5 m/s$ the turbine operated in a Reynolds dependent area. Because the turbine was not working at optimal conditions the velocity distribution across the wake was uneven and less energy was extracted from the turbine. Measurements were performed at $0,5D$ downstream of the rotor, both with and without additional tower. The movements of the tower shadow were not perceptible different compared to measurements at higher free stream velocities.

5.2 Future work

During the experiment questions asked in the beginning of the process were answered. The experiment found that the reason for the downshift of the rotational axis can be addressed the presence of the tower. However, there is some problems that would be of interest to investigate further.

For instance, it would be interesting to examine how strong the downshift influences the performance of the turbines further downstream in a wind farm arrangement. A wind tunnel experiment containing two turbines with additional tower, could be performed. C_p and C_T curves for the second turbine could be calculated and compared with equivalent experiments without the additional tower.

Turbulence measurements could probably capture the movement of the tower wake even better than velocity measurements. Thus, a similar experiment as the present could be performed, for example with Hot Wire as measurement instrument.

To be able to further investigate the influence of the free stream velocity, measurements at greater distances down the wake, at low wind tunnel speeds, could be performed. The experiment should be accomplished in a velocity range of independent Reynolds numbers.

Bibliography

[1] M.S. Adaramola and P-Å. Krogstad. Model tests of a horizontal axis wind turbine in yawed condition. *European Offshore Wind 2009 Conference and Exhibition*, September 2009.

[2] M.S. Adaramola and P-Å. Krogstad. Experimental investigation of wake effects on wind turbine performance. *Renewable Energy*, 36(8):2078–2086, August 2011.

[3] ASME. Test uncertainty. *American Society of Mechanical Engineers, New York*, Part 1(ASME PTC 19.1-1998), 1998.

[4] S. Barber, N. Chockani, and R.S. Abhari. Wind turbine performance and aerodynamics in wakes within wind farms. 2011.

[5] J. Bartl. Wake measurements behind an array of two model wind turbines. *Master's Thesis, NTNU Trondheim*, 2011.

[6] H. Blomhoff. Vindtunnelstudie av vaken nedstrøms for en vindturbin. *Project's Thesis, NTNU Trondheim*, 2011.

[7] T. Burton, D. Sharpe, N. Jenkins, and E. Bossanyi. *Wind energy: Handbook.* Wiley Online Library, second edition, 2001.

[8] A. Crespo, J. Hernandez, E. Fraga, and C. Andreu. Experimental validation of the upm computer code to calculate wind turbine wakes and comparison with other models. *Journal of Wind Engineering and Industrial Aerodynamics*, 27(1-3):77–88, January 1988.

[9] P.E. Eriksen. Wake of windturbines. *Internal paper, NTNU Trondheim*, 2011.

[10] P. Jain. *Wind Energy Engineering.* The McGraw-Hill Companies, first edition, September 2011.

[11] S.H. Kim, Y.J. Kang, R.S. Myong, T.H. Cho, Y.M. Park, and I.H. Choi. Calibration of a five-hole multi-function probe for helicopter air data sensors. *Int' 1 J. of Aeronautical and Space Sciences*, 10(2):43–51, November 2009.

[12] C. Kress, S. Barber, N. Chokani, and R. S. Abhari. Improved modeling of wakes: Experimental study and experimentally anchored model. *Laboratory for Energy Conversion, ETH Zurich.*

[13] P-Å. Krogstad. Modelltest av tidevannsturbin for kvalsundet. *MTF-Rapport 2002:5 (C)*, Juni 2002.

[14] P-Å. Krogstad and J.A. Lund. An experimental and numerical study of the performance of a model turbine. *Wind Energy*, 15(3):443–457, June 2011.

[15] K.M. Loland. Wind turbine in yawed operation. *Master's Thesis, NTNU Trondheim*, 2011.

[16] T. Maeda, T. Yokota, Y. Shimizu, and K. Adachi. Wind tunnel study of the interaction between two horizontal axis wind turbines. *Wind Engineering*, 28(2):197–212, 2004.

[17] J.F. Manwell, J.G. McGowan, and A.L. Rogers. *Wind Energy Explained Theory, Design and Application.* John Whiley & Sons Ltd., second edition, 2009.

[18] M. Méchali, R. Barthelmie, S. Frandsen, and PE Réthoré. Wake effects at horns rev and their influence on energy production. In *European Wind Energy Conference and Exhibition*, page 10, 2006.

[19] G.L. Morrison, M.T. Schobeiri, and K.R. Pappu. Five-hole pressure probe analysis technique. *Flow Measurement and Instrumentation*, 9(3):153–158, June 1998.

[20] V. Nelson. *Wind energy: Renewable Energy and the Environment.* CRC, 2009.

[21] C.F.R. Nowack. Improved calibration method for a five-hole spherical pitot probe. *Journal of Physics E: Scientific Instruments*, 3(1):21–26, 1970.

[22] Ø.V. Nygard. Wake behind a horizontal - axis wind turbine. *Master's Thesis, NTNU Trondheim*, 2011.

[23] F. Pierella. Wake of windturbines - internal paper. *Internal paper, NTNU Trondheim*, 2011.

[24] K. Rave, S. Teske, and S. Sawyer. Global wind energy outlook 2010. *Global Wind Energy Council [http://www.gwec.net]*, October 2010.

[25] E.P Rood and D.P. Telionis. September 1991 editorial on experimental uncertainty. *Journal of Fluids Engineering*, September 1991.

[26] B. Sanderse. Aerodynamics of wind turbine wakes. *Energy research Centre of the Netherlands, ECN-E-09-016*, 2009.

[27] H. Schümann. The interaction between wind turbines caused by their respective wakes. *Master's Thesis, NTNU Trondheim*, 2012.

[28] A.M. Talmon. A wind tunnel investigation into the effects of tower and nacelle on wind turbine wake flow. *TNO Division of Technology for Society*, Report 84-08479, 1984.

[29] A.M. Talmon. The wake of a horizontal axis wind turbine model, measurements in uniform approach flow and in a simulated boundary layer. *TNO Division of Technology for Society*, Report 85-01021, 1985.

[30] L.J. Vermeer, J.N. Sørensen, and A. Crespo. Wind turbine wake aerodynamics. *Progress in aerospace sciences*, 39(6-7):467–510, 2003.

[31] E.W. Weisstein. Root mean square. *Mathworld - A Wolfram Web Resource http://mathworld.wolfram.com/Root-Mean-Square.html*, 2011.

[32] A.J. Wheeler and A.R. Ganji. *Introduction to engineering experimentation*. Pearson/Prentice Hall, 2004.

[33] F.M. White. *Viscous Fluid Flow*. The McGraw-Hill Companies, third edition, 2006.

Appendix A

Uncertainty Analysis

To validate the results, it is necessary to perform an uncertainty analysis [25]. With certainty, the results must be located within a specific interval.

For each measurement 450 points were registered at 30Hz over 15 seconds. Besides the mean value, a rms value was also noted. This corresponds to the standard deviation of the mean velocity in each point [31]. Below, a procedure to calculate the uncertainty interval is present:

F is a function of n measured variables, which the uncertainty will vary about:

$$F = f(x_1, x_2....x_n) \tag{A.1}$$

From the measured values an uncertainty interval can be constructed, $\pm W$, where the mean value, by 95% certainty is located. W is defined as:

$$W = \sqrt{B^2 + (2S)^2} \tag{A.2}$$

B represents the systematic uncertainty attached to the individual measurement instrument and S represents the random uncertainty of the measured results.

The systematic uncertainty of the mean velocity component is calculated as:

$$B = \left(U^+ - U^-\right) \tag{A.3}$$

Where $\pm$ represents the upper and lower limit of the measured mean velocity component.

The random uncertainty, S, attached to the measurements is determined from:

$$S = \sqrt{\left[\sum \left(S_i \frac{\delta F}{\delta x_i}\right)^2\right]} \tag{A.4}$$

S_i is the standard deviation of each measured result, determined by the measured rms value, and $\frac{\delta F}{\delta x_i}$ is the sensitivity coefficient of the measurement of result F with respect to variable x_i.

The velocity components in the wake are determined from several instruments, hence the procedure of evaluating the uncertainty for each component is a comprehensive process. The systematic uncertainty for each instrument must be located and the random uncertainty for each measured point must be determined before an uncertainty interval can be constructed. Thus, an uncertainty analysis will only be performed for the free stream velocity, U_∞, about a certain measurement point.

A.1 Uncertainty analysis of the free stream velocity, U_∞

The free stream velocity in the tunnel is calculated from equation 3.3. The upper and lower limit of the velocity in the free stream are then determined from:

$$U_\infty^\pm = \sqrt{\frac{2 \times \triangle p_{contr}^\pm}{\rho^\pm \times \left(1 - \left(\frac{A_2}{A_1}\right)^2\right)}} \qquad (A.5)$$

The systematic uncertainty of the pressure transducer is assumed to be in the range of $\triangle p_{contr} \pm 1\% \times \triangle p_{contr}$.

The upper and lower limit of the density in the tunnel are calculated from values measured by the thermocouple, attached to the wind tunnel wall (see equation 3.9):

$$\rho^\pm = \frac{p_{atm}}{R_{spesific} T_{temp}^\pm} \qquad (A.6)$$

Where the systematic uncertainty related to the thermocouple is assumed to be $T_{temp} \pm 1\% \times T_{temp}$.

Calculating the upper and lower limit of the velocity value (equation A.5), the systematic uncertainty is (equation A.3): $B = 0,24 m/s$.

The random uncertainty of the contraction velocity is determined by the pressure transducer. The different terms in equation A.4 are calculated by the following expressions:

$$\frac{\delta U_\infty}{\delta \triangle p} = \sqrt{\frac{1}{2 \times \triangle p \times \rho \times \left(1 - \left(\frac{A_2}{A_1}\right)^2\right)}} \qquad (A.7)$$

$$S_{\triangle p} = 58,26 \times rms_{contr} \qquad (A.8)$$

The constant, $58,26$, is determined by the calibration of the pressure transducer, at the contraction section.

The random uncertainty is then calculated (equation A.4): $S = 0,062$

Finally, equation A.2 gives a 95% confidence interval about the free stream velocity: $U_\infty = (11 \pm 0,27) m/s$.

Appendix B

Risk assessment

Risk Assessment Report

Offshore Wind Tunnel

Project name	An experimental investigation of wind turbine wakes
Project leader	Lars Sætran
Unit	NTNU
HMS-coordinator	Bård Aslak Brandåstrø
Head of department	Olav Bolland
Placement	Strømningsteknisk laboratoriet
Room number	101C
Responsible for rig	Lars Sætran
Risk assessment performed by	Hedda Blomhoff, Lars Sætran

1 INTRODUCTION

In the present study, the wake behind a scaled horizontal axis wind turbine was investigated. The measurement instrument used in the experiments was a five-hole pitot probe. The experiments were performed at the Department of Energy and Process Technology, at the Norwegian University of Science and Technology, NTNU. A total risk assessment of the wind tunnel has previously been performed.

2 EVACUATION FROM THE EXPERIMENT AREA

Evacuate at signal from the alarm system. Evacuation from the laboratory takes place through the marked emergency exits to the meeting point, (corner of Old Chemistry, Kjelhuset or parking 1a-b.)

Action on rig before evacuation:

By evacuation, the wind tunnel shall be turned off by pressing the emergency stop button. All socket outlets, attached to the experiments, should be out before the operator returns to safety at the meeting point.

3 ASSESSMENT OF TECHNICAL SAFETY

3.1 HAZOP

The experiment set up is divided into the following node:

Node 1	Wind Tunnel

Attachments, scheme: Hazop mal

4 ASSESSMENT OF OPERATIONAL SAFETY

Assessment of operational safety ensures that established procedures cover all identified risk factors. It also ensures that the operators and technical performance have sufficient expertise.

4.1 Operation and emergency shutdown procedure

The operating procedure is a checklist that must be filled out for each experiment. Emergency procedure should attempt to set the experiment set up in a harmless state by unforeseen events.

Attachments: Procedure for running experiments

Emergency shutdown procedure:

If any risk events occur, the wind tunnel shall be turned off by pressing the emergency stop button. All socket outlets attached to the experiments, should be out before the operator returns to safety at the meeting point.

4.2 Training of operators

Before the experiments I learned about safety connected to the laboratory in general. I learned how to use the equipment's in a safe way and accomplished an HMS course online and by a guided tour in the laboratory.

Attachments: Training program for operators

4.3 Technical modifications

- Technical modifications made by the Operator

    ○ *The instruments placed outside the wind tunnel can be changed by the operator.*

- Technical modifications that must be made by Technical staff:

    ○ *Changes besides instrumentation placed outside the wind tunnel must be accomplished by technical personnel*

- What technical modifications give a need for a new risk assessment

    ○ *If changes affects the integrity of the wind tunnel a new risk assessment must be accomplished*

5 QUANTIFYING OF RISK - RISK MATRIX

The risk matrix will provide visualization and an overview of activity risks so that management and users get the most complete picture of risk factors.

ID nr	Activity-occurrence	Frequency-probability	Consequences	RV
1	*The rotor of the wind turbine comes off*	1	B	32

Conclusion:

The wind turbine is mounted in the wind tunnel. The tunnel is closed and the operator is placed outside the unit and is not exposed to risk.

6 CONCLUSION

The wind tunnel is a safe construction and a risk assessment report is already accomplished on the rig. The experiments were performed in controlled terms and no risk related events occurred.

Attachment to Risk Assessment report

Offshore wind tunnel

Project name	An experimental investigation of wind turbine wakes
Project leader	Lars Sætran
Unit	[SINTEF/NTNU]
HMS-coordinator	Bård Aslak Brandåstrø
Head of department	Olav Bolland
Placement	Strømningsteknisk laboratoriet
Room number	101C
Responsible for rig	Lars Sætran

NTNU   SINTEF

ATTACHMENT A - HAZOP MAL

Project:
Node: 1

Ref #	Guideword	Causes	Consequences	Safeguards	Recommendations	Action	Date Sign
	No flow	Power out	Experiment delayed		Restore power		31.05.2012 Heddar Blomhoff
	Reverse flow	N/A					
	More flow	Increase in flow velocity	Damage to equipment	Put up a sign	Put up a sign		"
	Less flow	Decrease in flow velocity	Damage to equipment	Put up a sign	Put up a sign		"

ATTACHMENT B - PROCEDURE FOR RUNNING EXPERIMENTS

Experiment, name, number:	Date/
An experimental investigation of wind turbine wakes	**Sign**
Project Leader:	30.05.2012
Lars Sætran	*(signature)*
Experiment Leader:	31.05.2012
Hedda Blomhoff	Hedda Blomhoff
Operator, Duties:	
Hedda Blomhoff	ll

	Conditions for the experiment:	Completed
	Experiments should be run in normal working hours, 08:00-16:00 during winter time and 08.00-15.00 during summer time. Experiments outside normal working hours shall be approved.	x
	One person must always be present while running experiments, and should be approved as an experimental leader.	x
	An early warning is given according to the lab rules, and accepted by authorized personnel.	x
	Be sure that everyone taking part of the experiment is wearing the necessary protecting equipment and is aware of the shutdown procedure and escape routes.	x
	Preparations	**Carried out**
	Post the "Experiment in progress" sign.	x
	Startup procedure (Wind tunnel)	x
	During the experiment	
	Control of temperature, pressure e.g.	x
	End of experiment	
	Shut down procedure	x
	Remove all obstructions/barriers/signs around the experiment.	x
	Tidy up and return all tools and equipment.	x
	Tidy and cleanup work areas.	x
	Return equipment and systems back to their normal operation settings (fire alarm)	x
	To reflect on before the next experiment and experience useful for others	
	Was the experiment completed as planned and on scheduled in professional terms?	x
	Was the competence which was needed for security and completion of the experiment available to you?	x
	Do you have any information/ knowledge from the experiment that you should document and share with fellow colleagues?	x

ATTACHMENT C - TRAINING OF OPERATORS

Experiment, name, number:	Date/
An experimental investigation of wind turbine wakes	**Sign**
Project Leader:	30.05.2012
Lars Sætran	*[signature]*
Experiment Leader:	31.05.2012
Hedda Blomhoff	Hedda Blom-
Operator	hoff
Hedda Blomhoff	˅

	Knowledge to EPT LAB in general	
	Knowledge about access, routines and rules and working hours in the Lab	˅
	Knowledge about the evacuation procedures	˅
	Knowledge about the activity calendar for the Lab	˅
	Knowledge to the experiments	
	Knowledge about procedures for the experiments	˅
	Knowledge about emergency shutdown	˅
	Knowledge about the nearest fire and first aid station	˅

Operator	**HMS responsible**
Date 31.05.2012	Date 30/05-2012
Signature Hedda Blomhoff	Signature *[signature]*

ATTACHMENT D - FORM FOR SAFE JOB ANALYSIS

HMS aspekt	Ja	Nei	Ikke aktuelt	Kommentar / tiltak	Ansv.
Dokumentasjon, erfaring, kompetanse					
Kjent arbeidsoperasjon?	x				HB
Kjennskap til erfaringer/uønskede hendelser fra tilsvarende operasjoner?	x				\\
Nødvendig personell?	x				\\
Kommunikasjon og koordinering					
Mulig konflikt med andre operasjoner?		x			\\
Håndtering av en evnt. hendelse (alarm, evakuering)?		x			\\
Behov for ekstra vakt?		x			\\
Arbeidsstedet					
Uvante arbeidsstillinger?		x			\\
Arbeid i tanker, kummer el.lignende?		x			\\
Arbeid i grøfter eller sjakter?		x			\\
Rent og ryddig?	x				\\
Verneutstyr ut over det personlige?		x			\\
Vær, vind, sikt, belysning, ventilasjon?	x				\\
Bruk av stillaser/lift/seler/stropper?		x			\\
Arbeid i høyden?		x			\\
Ioniserende stråling?		x			\\
Rømningsveier OK?	x				\\
Kjemiske farer					
Bruk av helseskadelige/giftige/etsende kjemikalier?		x			\\
Bruk av brannfarlige eller eksplosjonsfarlige kjemikalier?		x			\\
Må kjemikaliene godkjennes?		x			\\
Biologisk materiale?		x			\\
Støv/asbest?		x			\\
Mekaniske farer					
Stabilitet/styrke/spenning?		x			\\
Klem/kutt/slag?		x			\\
Støy/trykk/temperatur?	x			The wind tunnel produced a lot of noise, therefore earplugs were applied	\\
Behandling av avfall?		x			\\
Behov for spesialverktøy?		x			\\
Elektriske farer					
Strøm/spenning/over 1000V?		X			\\
Støt/krypstrøm?		X			\\
Tap av strømtilførsel?		X			\\
Området					
Behov for befaring?		X			\\

Merking/skilting/avsperring?	x			Experiment in progress sign was applied	ll
Miljømessige konsekvenser?		x			l\
Sentrale fysiske sikkerhetssystemer					
Arbeid på sikkerhetssystemer?		x			\\
Frakobling av sikkerhetssystemer?		x			l\
Annet					

NTNU SINTEF

- **VEDLEGG J APPARATURKORT UNITCARD**

Apparatur/unit

Dette kortet SKAL henges godt synlig på apparaturen! *This card MUST be posted on a visible place on the unit!*

Faglig Ansvarlig (Scientific Responsible) Lars Sætran	**Telefon mobil/privat** (Phone no. mobile/private) 48409999
Apparaturansvarlig (Unit Responsible) **Lars Sætran**	**Telefon mobil/privat** (Phone no. mobile/private) 48409999
Sikkerhetsrisikoer (Safety hazards) **No safety hazards as long as doors are closed properly**	
Sikkerhetsregler **Operate rig only after doors are properly closed. If it is necessary to be inside the wind-tunnel during operation the minimum safety precaution is Safety-glasses.**	
Nødstopp prosedyre Emergency stop is located right next to the fan. Push emergency stop when necessary.	

Her finner du (Here you will find):

Prosedyrer (Procedures) In manual next to test rig.	
Bruksanvisning (Users manual) In manual next to test rig	

Nærmeste (nearest)

Brannslukningsapparat (fire extinguisher) In hall	
Førstehjelpsskap (first aid cabinet) In hall	

NTNU
Institutt for energi og prosessteknikk

Dato 12/10-2011

Signert *Olav Bolland*

SINTEF Energi
Avdeling energiprosesser

Dato

Signert

5

- **VEDLEGG K FORSØK PÅGÅR KORT**

Forsøk pågår!
Experiment in progress!

Dette kort skal settes opp før forsøk kan påbegynnes This card has to be posted before an experiment can start

Ansvarlig / Responsible Lars Sætran	Telefon jobb/mobil/hjemme 48409999
Operatører/Operators Lars Sætran. Arnt Egil Kolsatd ++ properly trained operators	Forsøksperiode/Experiment time(start – slutt) Permanent
Prosjektleder Lars Sætran	Prosjekt Stor vind-tunell

Kort beskrivelse av forsøket og relaterte farer
Short description of the experiment and related hazards

The wind-tunnel will/can be used for a wide variety of experiments. The main tunnel is an enclosed stand-alone unit where the operator and observers normally are on the outside of the see-through wall. If need be that one has to be inside during some tests, the minimum safety precaution is Safety-glasses !

NTNU Institutt for energi og prosessteknikk	SINTEF Energi Avdeling energiprosesser
Dato 12/10 – 2011	Dato
Signert	Signert

6